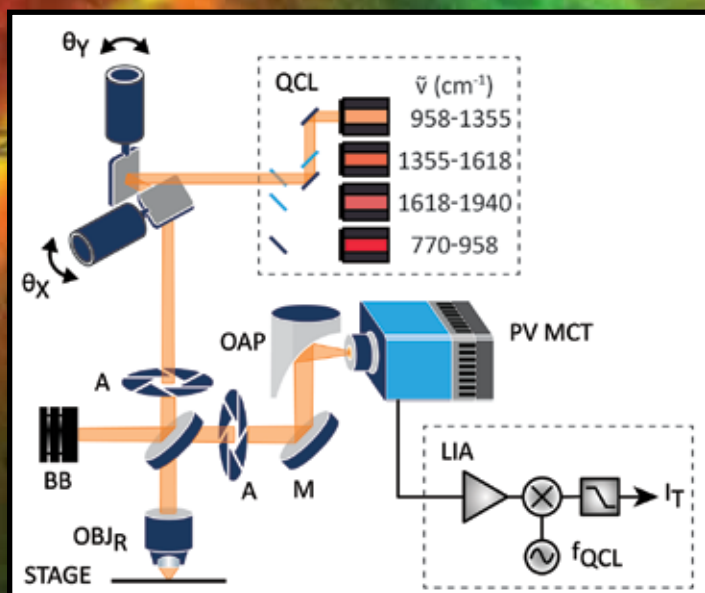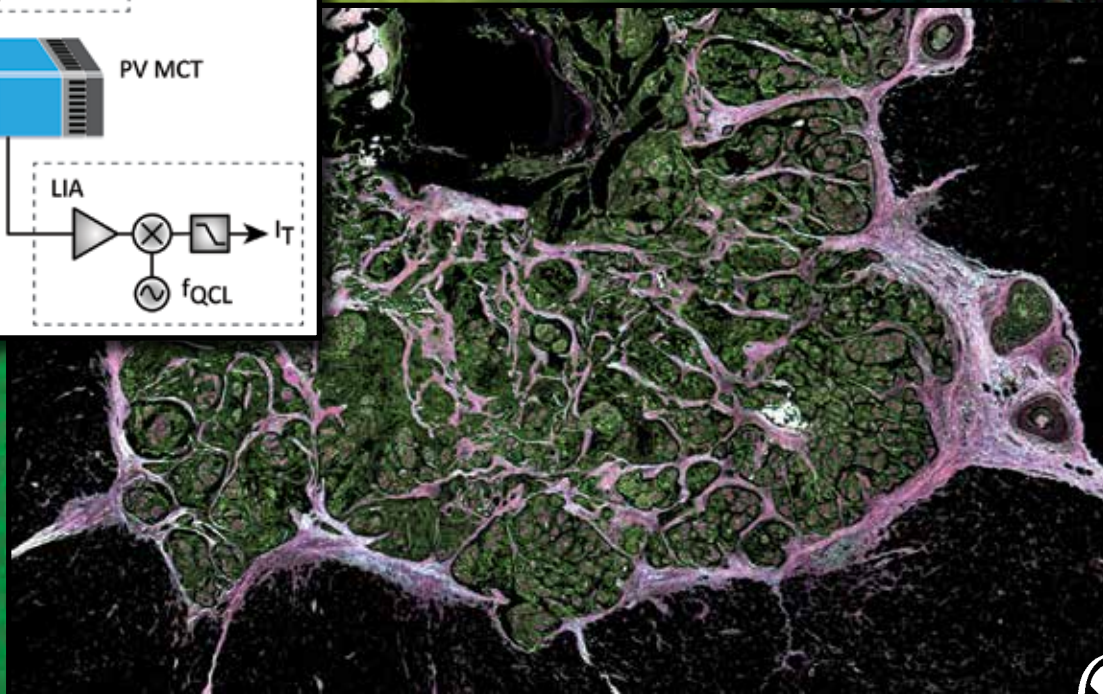# Applied Spectroscopy®

An International Journal of Spectroscopy

Design Considerations for Discrete Frequency Infrared Microscopy Systems

SOCIETY for APPLIED SPECTROSCOPY
hv
www.s-a-s.org

Design Considerations for Discrete Frequency Infrared Microscopy Systems

Yamuna Phal[1,2], Kevin Yeh[2], and Rohit Bhargava[1,2,3,4]

Abstract

Discrete frequency infrared chemical imaging is transforming the practice of microspectroscopy by enabling a diversity of instrumentation and new measurement capabilities. While a variety of hardware implementations have been realized, design considerations that are unique to infrared (IR) microscopes have not yet been compiled in literature. Here, we describe the evolution of IR microscopes, provide rationales for design choices, and catalog some major considerations for each of the optical components in an imaging system. We analyze design choices that use these components to optimize performance, under their particular constraints, while providing illustrative examples. We then summarize a framework to assess the factors that determine an instrument's performance mathematically. Finally, we provide a validation approach by enumerating performance metrics that can be used to evaluate the capabilities of imaging systems or suitability for specific intended applications. Together, the presented concepts and examples should aid in understanding available instrument configurations, while guiding innovations in design of the next generation of IR chemical imaging spectrometers.

Keywords

Infrared microscopy, IR microscopy, design of IR microscopes, optical design, design considerations, performance metrics, quantum cascade laser, spectroscopy, chemical imaging, Fourier transform infrared, discrete frequency infrared

Date received: 5 February 2021; accepted: 9 April 2021

Introduction

The design and development of modern optical imaging has advanced through theory, experimental advancements, and extensive validation over centuries. Meanwhile, the numerous advantages offered by imaging in the mid-infrared (IR) spectral region are only starting to be realized and have been receiving considerable recent attention in the microscopy community. IR imaging not only allows for morphological analyses similar to optical imaging, but additionally facilitates an understanding of the molecular structure of multi-component materials through spectral fingerprinting. The major bottlenecks in advancing IR imaging are technological barriers such as underdeveloped camera technology, fundamental differences with optical microscopy such as the incompatibility with common glasses, as well as practical challenges such as high per unit costs of components due to relatively fewer users compared to optical imaging. Another critical difference between optical and IR imaging technology is the need for computationally intensive post-processing techniques to understand and interpret spectroscopic data. Finally, working at wavelengths that cannot be seen poses well-recognized experimental barriers. With the recent advances in theoretical understanding, greater tractability in computational complexity, and declining costs of custom fabrication, an assortment of IR spectroscopic imaging approaches is becoming more accessible. Although proposed nearly 70 years ago,[1,2] IR imaging is now being increasingly realized as a viable label-free complement to optical microscopy. This review focuses on coalescing important aspects in these technological developments and providing a compendium for recent progress in discrete frequency infrared (DFIR) imaging.

[1]Department of Electrical and Computer Engineering, University of Illinois at Urbana-Champaign, Urbana, USA
[2]Beckman Institute for Advanced Science and Technology, University of Illinois at Urbana-Champaign, Urbana, USA
[3]Departments of Bioengineering, Mechanical Science and Engineering, Chemical and Biomolecular Engineering, and Chemistry, University of Illinois at Urbana-Champaign, Urbana, USA
[4]Cancer Center at Illinois, University of Illinois at Urbana-Champaign, Urbana, USA

Corresponding author:
Rohit Bhargava, Beckman Institute for Advanced Science and Technology, University of Illinois at Urbana-Champaign, 405 N Mathews Ave., Urbana, IL 61801-2325, USA.
Email: rxb@illinois.edu

A key step toward making IR spectroscopic microscopy feasible was the advent of Fourier transform (FT) spectrometers,[3] providing speed, sensitivity, and data handling capability. Driven by advances in computing, theory, design, myriad applications, and new ideas, the field diversified beyond Fourier transform infrared (FT-IR) microscopy.[4] Early modification of FT-IR imaging used custom-designed filters[5–7] to image narrow bandwidths; as opposed to FT-IR imaging that measured wide bandwidths simultaneously, and this class of imaging was termed discrete frequency IR (DFIR) imaging. The accelerated pace of progress in DFIR instrumentation has been largely due to the ready availability of quantum cascade lasers (QCLs),[8–10] which provides a bright, collimated, narrow linewidth, and reliable source that obviates the need for a spectrometer. Now more fundamental changes are afoot. For nearly half a century, the major design direction of IR microscopes followed the folding reflective optical geometries seen in telescopes. In contrast, refractive optics that were carefully machined from an extremely limited selection of fragile IR transparent materials were more popular for thermal cameras. With modern fabrication capabilities, the diversity of refractive, reflective, and flat lenses[11,12] is becoming extensively available. Similarly, advances in narrow band gap semiconductor technology have allowed IR detectors to integrate detection and readout capabilities on a single chip. These advances promise significant upcoming technologies that will combine new sources, spectrometer designs, microscopy formats, and detectors. But we also need to consider challenges that arise from a still emerging scientific understanding of image formation processes, a lack of codification of best practices to optimally using technological advances in components and matching applications to instrumentation capabilities for a rapid translation to practice. We present here a collated set of important developments, trends, trade-offs, and insights into potential directions. Understanding options and possible configurations will help to form a framework that promotes continued progress in IR microscopy. Together, these factors will aid in understanding the context and effect of recent and upcoming advances in DFIR imaging to guide new innovations in applied spectroscopy.

The dominant mode of recording absorption of IR light by a sample is to measure the residual IR light intensity passing through a sample and computing the loss relative to a stored calibration. With significant practical importance, this technique is also currently the fastest and most sensitive in terms of spectral quality of quantifying IR absorption. We focus our review on the class of instruments limited to this mode of detection. Detection of the absorbed light, of course, is not directly possible but the consequence of absorption in increasing the local temperature or physical dimensions can be sensed. Typically, non-IR detection methods have been demonstrated to detect the effects of absorption, these include mechanical scanning probes,[13–25] using a secondary optical probe beam,[26–35] and ultrasound transduction.[36,37] These hybrid IR systems can estimate absorption, but the relatively weak effects require increased sensitivity.[38–40] Due to the multitude of detection modes and use of sensitivity enhancement aids such as lock-in amplification or interferometry, the scope of design considerations becomes very large and is best left for each detection modality separately. We describe here systems that directly measure IR light using IR compatible optics and detector assemblies, essentially through an instantaneous acquisition. We focus on missing descriptions of a methodical design approach and consider advances in each component, while identifying potential paths for continued improvements in DFIR imaging.

Instrument Design

Traditionally, IR microscopes have relied on designs that illuminate the sample by modulation of a spectrometer's output in both time (either sequential frequency scanning or interferometry) and space (either using an aperture scan or spatially multiplexed recording). Older generation designs were based on optically dispersing light from a thermal source using a prism or grating and blocking out unwanted frequencies to measure individual frequency components to build up a spectrum. To obtain spatially resolved data, light was restricted using an aperture in the microscope's beam path to illuminate a small area of controlled dimensions on the sample.[1,41–44] Remarkable data could be obtained from these systems considering that most of the light of the broadband source was eliminated by the spectral filters and significantly reduced further by the spatial aperture. While demonstrative examples could be recorded, the low signal-to-noise ratio (S/N), long acquisition times, lack of a spatial rastering mechanism, and absence of electronic data management ultimately restricted applications to examination of small samples or single microscopic regions. A dominant limiting factor was the need to span a large bandwidth with the source ($\sim$hundreds of wavenumbers) balanced by the requirement to measure only a narrow bandwidth ($\sim$1–10 cm^{-1}) for spectral analyses. The addition of a multi-element detector can result in many spectral channels being acquired simultaneously, with each pixel recording a different spectral bin.[45,46] Even with a multiplexing detection advantage, however, dispersion techniques are limited in the collection of higher resolution or S/N since light throughput decreases significantly with the spectral bin width.[47] Thus, imaging or even sequential point mapping is often impractical by restricting the broadly emitting, but weak globar source.

The quest for higher S/N, to enable more sensitive analyses and faster recording in IR spectroscopy, is well documented and the application of interferometry to record high-precision absorption measurements was a breakthrough that was enabled by advances in instrumentation,

computing (of the fast Fourier transform, or FFT), and data handling capability.[48] FT-IR spectrometers improved upon the limitations of scanning monochromators by measuring spectral elements simultaneously to provide an S/N improvement equal to the square root of the number of spectral points scanned (Fellgett advantage). The improvement was further compounded by eliminating small slits needed to reject the majority of transmitted light in dispersive systems (Jacquinot advantage), albeit with large apertures and small resolution. These improvements in S/N and spectral acquisition speed not only made FT instruments the standard for spectrometry but also enabled practical spectroscopic measurements for samples on a microscopic scale.[3,49–54] A notable advance to address the low power was the use of synchrotrons[55–62] that provided a collimated, compact, and bright source[63] for unprecedented spatial and spectral quality from microscopic samples.[64–68] The use of array detectors with different spectrometer operation modes[69–74] was another turning point and led to the most recognizable imaging formats available—use of an array detector on an IR microscope coupled to an interferometer and broadband source. The multiplexed detection advantage from using even poor-quality detectors was large enough to provide wide spatial coverage and acceptable S/N for many applications.[75–89] The relative advantages of array detection compared to point-scanning[90,91] are active areas of interest in the field of IR microscopy, just as it is in other molecular microscopies such as fluorescence. Nonetheless, optimizing the S/N of point detectors continues to remain a major theme.[92,93] Another major milestone was the development of instrumentation with a small, multiplexed detection scheme using a sensitive linear array detector to balance spatial coverage with spectral S/N.[94] While providing slower imaging speeds, the molecular analytical capability of this system was higher than any other reported FT-IR imaging system. Such large array detector-based systems focused on acquiring measurements in reaction kinetics,[95,96] either in time-resolved mode[97] or in multiplexed mode.[98,99] Continued improvements over the FT-IR spectrometer–microscope framework in optical design primarily drove improvements in technology,[100–102] with significant efforts being focused on increasing imaging quality using a solid immersion lens or attenuated total reflection,[80,103–108] modeling, and simulation[109] as well as advances in instrument design.[74,110–113] Synchrotron-focal plane array combinations continued to provide exceptional capability[74,111,114] and table top systems now routinely provide high-definition IR imaging.[112,115–123] While it is not our intent here to provide a comprehensive coverage of the development of IR imaging technology, these representative examples serve to show how a diversity of components can lead to advances and different optimal combinations that are useful for specific applications but involve design trade-offs. The recent past has seen two major changes that merit special attention, the evolution of the IR microscope and the availability of QCLs.

Among all these changes, the basic framework of the IR microscope has changed little. IR microscopes were nearly entirely designed using lenses with reflective geometries to overcome chromatic aberration across the broad bandwidth of FT spectrometers, a necessity arising from the need for the Fellgett advantage. An example configuration is as shown in Fig. 1a. Folding the light path throughout the instrument is necessary with these designs and is also needed to provide sampling flexibility. However, it also results in a relatively larger footprint and substantial energy is lost as the incoherent light is propagated over long distances and reflected by multiple surfaces. Reflective geometries offer an inevitable trade-off to refractive designs with much shorter optical path lengths. However, all IR transparent lens materials exhibit a high dispersion and reduced throughput when compared to reflective mirrors. For high magnification imaging in particular, the effects of dispersion in refractive materials becomes even more pronounced resulting in out-of-focus spectra and images. Due to the wide spectral bandwidth that needs to be measured, FT-IR imaging is reliant on and highly suited to reflective Schwarzschild objectives, which have a simple reflective design that is also corrected for primary third-order aberrations. However, it is unclear whether the same lenses need to be used (and the drawbacks tolerated), even with a greater understanding of their effects on recorded spectra,[124–130] as new source technologies and optical designs emerge. Thus, it is timely to consider the entire imaging framework while changing the source–spectrometer for instance. The availability of new designs and new components is profoundly synergistic, and it is essential to thoroughly comprehend this interplay.

Perhaps the most significant recent development for IR microscopy has been the use of QCLs as sources to enable DFIR spectroscopic imaging as an alternative technology.[132,133,135–141] Compared to the classical FT systems, these designs have demonstrated significant gains in speed as well as competitive resolution and S/N when normalized for acquisition times. Many of these gains can be attributed to the narrowband high intensity properties of QCLs, as well as their discrete tunable emission, which allow for improved measurement efficiency and increased S/N. At the same time, these lasers are safe for most materials given that absorption is a very strong contrast mechanism and does not need very high illumination intensity. With proper instrument design, safe and nondestructive imaging is possible.[142,143] In the last decade, multiple optimal designs based on widefield[132,133,136–138,144] and point-scanning[135,140,141,145] configurations were developed, each with their own advantages and disadvantages, depending on the specific research question and the experimental scope. Collectively, the prior development of FT-IR techniques indicated and provided insights into the critical role
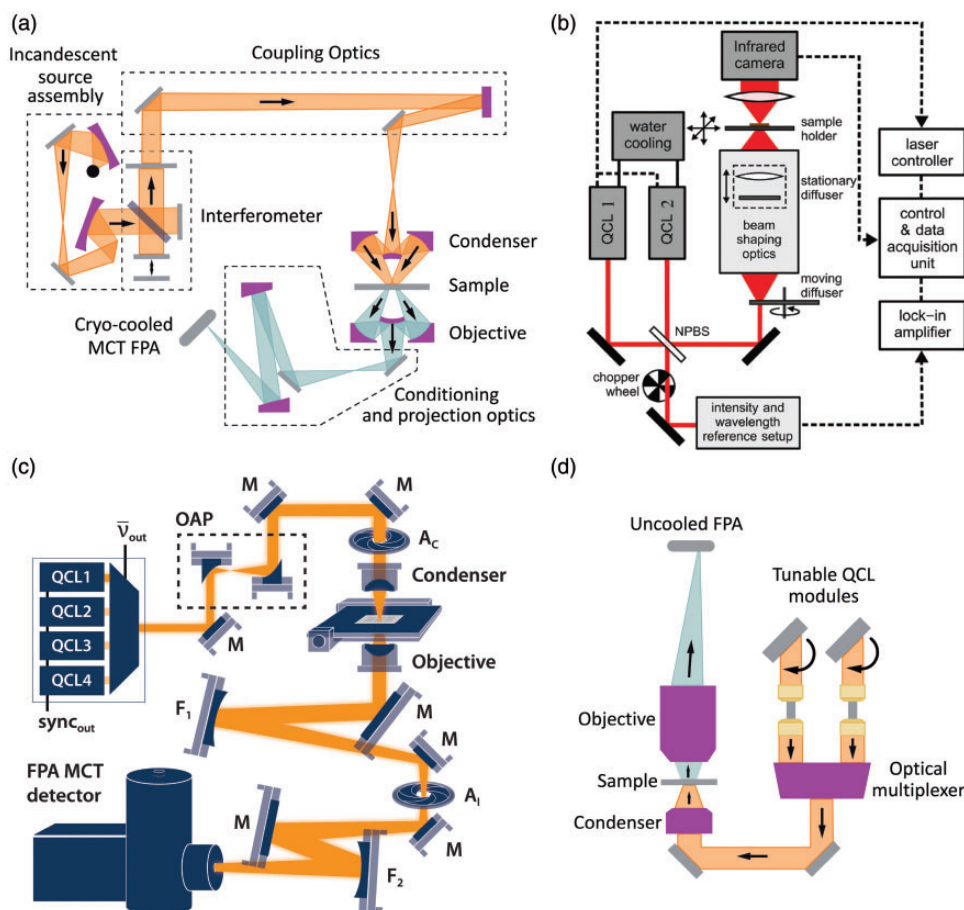
Figure 1. Widefield IR spectroscopic imaging instruments. (a) Fourier transform infrared (FT-IR) imaging microscope. Reproduced with permission from Rowlette et al.[131] Copyright 2021 Daylight Solutions Inc. Multiple DFIR imaging configurations have been reported with unique features: (b) Using a high numerical aperture (NA) refractive lens in an inverted transmission configuration to improve the resolution. The design was further synchronized with a high-frame rate focal plane array (FPA), while reducing illumination non-uniformity using high-speed laser tuning across the spectral range. Reproduced with permission from Yeh et al.[132] Copyright 2014 American Chemical Society. (c) Laser illumination is homogenized by a rapidly rotating diffuser[133] to reduce the laser speckle for widefield recording. Reproduced with permission from the Schonhals et al.[134] Copyright 2018 Wiley-VCH. (d) Commercial systems have enhanced accessibility of laser-based DFIR microscopy. Reproduced with permission from Rowlette et al.[131] Copyright 2021 Daylight Solutions Inc. These illustrations are presented for conceptual purposes only, with representations of major components, and are not intended to serve as a comprehensive schematic.

played by the design choices and the iterative design process. However, the transition to DFIR modalities now requires re-evaluating the development choices by revisiting this process with new rigorous and methodical design rationales that are explicitly tailored for DFIR instruments.

The first reports of QCL-based DFIR imaging systems[133] were in both the point-scanning and widefield modes, but closely followed the existing FT-IR microscope designs. As discussed previously, these microscopes were specifically tuned for a large incoherent source and replacing the source with a coherent narrow beam, presented illumination difficulties. However, by switching to refractive lenses with a high numerical aperture (NA), originally designed for fiber collimation, higher focusing powers were attainable, while maintaining acceptable image quality within a small

field of view (FOV). Widefield designs,[132,145] as shown in Fig. 1b, demonstrated imaging capabilities that were more than an order of magnitude faster than what was previously achievable. The combination of a QCL and high-speed mercury–cadmium–telluride (MCT) or HgCdTe focal plane array (FPA) could acquire hyperspectral images in seconds. Other designs incorporating stock compound IR lens assemblies, often termed as close-up lenses, as shown in Fig. 1c, offered wider FOV at the cost of resolving power,[131] while custom-designed compound IR objectives, as shown in the commercial system illustrated in Fig. 1d, achieved both a relatively high NA while maintaining a wide FOV,[131] but required larger format thermal cameras with slower frame rates. While successful in providing large volumes of data rapidly, widefield imaging configurations with

coherent sources are inherently subject to speckle arising from scattering in the optical train that compromises both morphological and spectral fidelity. Attempts to mitigate these issues and reduce the effect of laser speckle and coherent interference were developed, incorporating techniques such as spectral averaging,[132] rotating diffusers,[133,134,137] and time-delay integration,[139] but always at an expense of considerably increased acquisition time. We anticipate that increases in output power, wider tuning in single chips, greater wavelength ranges, and higher stability of turnkey QCL systems will emerge to drive innovations in IR imaging design in the near future.

Compared to FT-IR imaging and widefield DFIR microscopes, point-scanning confocal configurations have drastically improved the resolution and noise performance of IR microscopy. In these systems, a focused on-axis beam of light illuminates a single point, whose dimensions are determined by the optical configuration, and light is collected onto an aperture in a conjugate image plane after interaction with the sample.[135,140,141,145] Point-scanning designs largely eliminate speckle seen in widefield illumination. While superficially it may seem that the process of point-by-point mapping of a sample in DFIR point-scanning configuration cannot compete in speed with the multiplexed advantage of large format cameras, improvements in S/N due to a higher intensity and absence of coherence-induced artifacts are clear advantages. While the former results in larger signal value, the latter reduces noise, leading to shorter dwell times for a given S/N requirement. Due to these factors, the point-scanning technique is a preferred approach for applications requiring high-quality data and is the current gold standard in terms of precision and accuracy. When normalized for S/N, following the square root relation with time, the scanning design substantially outperforms widefield designs in total acquisition speed.[135] By far, the laser scanning systems offer the best choice in terms of

acquisition times and S/N, but the optical design has increased complexity with scan lenses, telecentric lenses, and infinity-corrected objectives, each containing many refractive elements.[135] In a laser scanning system, the maximum scan rate of the galvo controller drive limits the frame rate of images. For a stage or objective scanning system, the scanning speed of the relatively larger object limits the frame rate. Regardless, a trade-off exists between dwell time per pixel (or acquisition times) and S/N. Ultimately, applications determine the precise trade-offs that are acceptable in the design of an instrument.

Laser scanning confocal microscopy, where the laser beam is steered using precise control of fast mirrors, is a common modality for visible light microscopy. However, due to the unavailability of broadly corrected compound optics, it has not been a practical approach for broadband IR microscopy. Scanning optics designed for fixed wavelength IR lasers, e.g., CO_2 lasers for laser cutting, are not suitable for spectroscopic microscopy. Thus far, reported IR scanning systems rely only on on-axis illumination by either sweeping the objective lens mounted on a fast-moving platform over the sample or by keeping the lens fixed and moving the sample instead (Figs. 2a and 2b, respectively). The speed of these systems highly depends on the mass of the objective assembly or the sample carrier, which must rapidly accelerate and change directions over each scan pass. In either case, keeping the sample stationary minimizes the perturbation to the specimen, or keeping the optics stationary helps in maintaining consistent optical path length while minimizing inadvertent beam deflection and drift on the detector. To maintain overlap of the tightly focused illumination and detection focal volumes, especially for high resolution systems where these focal volumes are on the order of a few microns, it becomes convenient for both illumination and detection to share a common optical assembly. Instruments with epi-illumination geometries
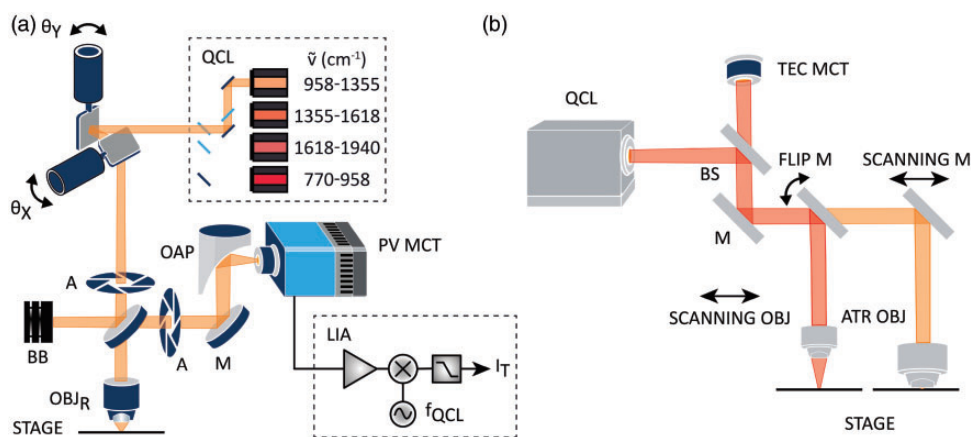
Figure 2. DFIR imaging by raster scanning a focused point illumination by (a) fixed objective and beam or stage scanning, or (b) a scanning objective assembly with a second arm providing attenuated total reflection (ATR) option for higher resolution imaging using a solid immersion lens in contact with the sample.[146]

focus light on the interface between the sample and the reflective substrate while collecting the reflected light after it passes through the sample a second time. The intrinsic ability to maintain alignment typically allows for such geometries to achieve better image and signal quality, but only if the system can maintain focus on the sample–substrate interface. The errors in tracking the interface are magnified by a factor of two, due to the double pass optical path through the sample. Overall, selecting the right modality requires stringent trade-off analysis during the design phase of the development regarding, for instance, the desired choice of technology and the development time versus the functional requirements of the system.

Once the specifications and performance criteria are established, designing the microscope involves a balance between the instrument functionality, compactness, performance, and cost. Optical design software, including CODE V, Zemax, OSLO, and FRED, provide optimization tools and quantitative performance estimations for conceptual optical systems. These tools can be used to design innovative multi-element optical layouts, corrected for most third-order aberrations over a broad spectral range, as would be required for developing widefield imaging microscopes. However, as these complex compound objectives have limited commercial availability in the IR spectral regime, point-scanning configuration is the preferred, feasible, and cost-effective approach employed to develop purpose-built DFIR microscopes. In this work, we focus on the major design decisions that are needed in the building of a custom DFIR microscope that meets the typical functional requirements. Broadly, the framework can be broken down into selection of three major modules, namely, the IR source, a high-speed low-noise IR detector, and IR optical elements, which taken altogether contribute to optimizing the optical design.

Infrared Source

Traditionally, thermal broadband sources, most commonly the globar, a heated silicon carbide rod, have been used in IR microscope design due to their simplicity, robustness, and low cost, excellent source-detector spectral matching.[4] Using such sources was beneficial with single-element detectors for bulk spectroscopic applications, where the photon flux is high. However, for microscopy applications, a much higher photon flux is desirable for increased S/N due to the use of apertures and smaller detectors. Synchrotron sources[3,64,91,147–149] are high-energy particle accelerators that produce intense light beams. Although widefield imaging with synchrotron sources demonstrated an improved S/N and spatial resolution over traditional FT-IR with a globar source,[110] this required access to a large synchrotron facility, presenting cost and accessibility challenges for widespread adoption.

The availability of the mid-IR femtosecond oscillators, such as optical parametric generators (OPG) and optical parametric oscillators (OPO), introduced new options for broadband coherent mid-IR sources. The light emission in OPG and OPO-based frequency combs is based on non-linear parametric optical frequency conversion of the incident beam into output beams of lower frequency determined by the phase matching condition. Discrete frequency modulation combs have been successfully demonstrated as efficient chip-scale devices with low power consumption.[150–152] With wide bandwidth, wavelength-independent spectral resolution, and high incident flux, these sources proved to have substantial advantages over traditional thermal emitters allowing for reasonable acquisition times, as well as better sensitivity and resolution.[153,154] However, their high cost has not yet made them practical for applications outside of fundamental research. Another limiting factor in the extensive acceptance of this technology is the shot-noise dominated performance of the sources in the IR regime. For imaging applications with reasonable S/N requirements, the choice of sources remains a pre-eminent challenge. An alternative to frequency combs are wide coherent mid-IR supercontinuum sources that are based on pumped dispersion-engineered fibers, so that strong nonlinear interactions produce broadband output with high brightness and low output noise.[155–157] Semiconductor laser sources such as vertical cavity surface-emitting lasers (VCSELs), which are coherent sources with high S/N, offer unprecedented advantages of low power consumption, narrow linewidth, single-fundamental-mode, and high wavelength tunability.[158] Initially limited to near-IR wavelengths, recent studies have extended spectral emissions to longer wavelengths, up to over $5\,\mu m$, with a high beam quality and a significantly higher power output up to 6.7 W.[159] However, commercial-grade VCSELs are not yet available in the mid-IR wavelength range, but the increasing need for compact, portable, and affordable gas sensors is spurring demand for energy-efficient semiconductor sources of mid-IR light.[160] Invention of VCSELs in the mid-IR range with continuous and pulsed mode operation is a significant step with the possibility of covering the molecular fingerprint region. Intrinsically, low-powered, portable, and inexpensive VCSEL-based chemical imaging systems offer a great potential for deployable microscopes in the future.

The recent advances in band-structure engineering of semiconductor lasers have advanced IR microscopy with the emergence of interband cascade lasers (ICL) and QCLs that are composed of a repeated stack of multiple quantum well heterostructures. As opposed to a diode laser in which the transitions occur between the conduction band and valence band of the semiconductor material, the emission is achieved through the use of interband or intersubband lasing transitions. ICLs are based on hybrid alloy substrates such as InAs, GaSb, AlSb, which are very

promising for compact and low power consumption applications in the 3–6 μm spectral range.[161,162] Alternatively, QCLs are based on III–V semiconductors and their alloys, such as GaAs–AlGaAs and InGaAs–InAlAs–InP, and utilize epitaxially grown quantum wells that contain electrons in lasing states. The above-mentioned lasers can be built in either a simple distributed feedback (DFB) configuration or an external cavity (EC) configuration with wide-tuning range capability. Very similar to the Fabry–Perot lasers in their operation, a DFB design uses a waveguide in combination with a distributed Bragg reflector (DBR) that forces single mode operation of the laser and exhibits a narrow emission linewidth. The DFB arrays provide the most widely tunable lasers,[163] but the coupler losses increase with the number of DBR lasers and there is a trade-off between the tuning range and the output power.[164] Alternatively, through insertion of the wavelength selective elements such as an external grating in the laser cavity, the EC configuration permits operation in a single mode, which is not as sensitive to temperature variations. By careful engineering and design of the quantum well depths during the fabrication process, lasing can be achieved at wavelengths as short as 2.75 μm[165,166] and as long as 161 μm,[167] with predominant interest concentrated in the mid-IR (3.5–12.8 μm) region of the spectrum. Frequency-selective optical feedback is obtained through diffraction gratings in either the Littrow[168] or Littman–Metcalf[169] configurations, which allows ECLs to achieve narrow linewidth and remarkable tunability.[170] With numerous advantages ranging from broad wavelength tunability, extreme narrow single mode operation, and spectral range extending between 5 and 24 μm, EC-QCLs are an ideal source for mid-IR imaging systems. The majority of new DFIR microscope designs rely on the EC-QCL. These QCLs have single mode emission and allow broad tunability with high spectral resolution, opening up a wide range of possibilities for fast and highly customized imaging applications.[162] The de facto standard today is four QCL modules multiplexed together as a single turnkey system, in order to cover the full biochemical fingerprint region spanning from 800 to 1900 cm^{-1}. It is a vital spectral regime for biological analysis and allows chemical identification and examination of complex tissues and heterogeneous samples.[4,171,172] The laser beam characteristics, including the intensity profile, divergence, and coherence, are important features to keep in mind during the selection process.

Unlike thermal emitters such as globars, QCL sources are intrinsically polarized and are coupled with high intensity illumination, making them an effective candidate for spectroscopic polarimetry[173,174] and vibrational circular dichroism[175] applications with high S/N and high spatial localization measurements. Hence, another performance merit for lasers, specifically for polarization imaging, is the degree of polarization of the output beam. Additionally, in many imaging applications, the most important laser beam

characteristic is the intensity of the output beam, which is related to the beam power, the cross-sectional area, and the beam divergence in the sample plane. Usually, a focused laser beam with a small divergence of ~3 mrad and a high degree of temporal and spatial coherence is preferable. In Fig. 3, we characterize an example laser system that comprises of four laser modules, covering the wavenumber range from 780 to 1850 cm^{-1} (12.8–5.4 μm). Moreover, hyperspectral measurements require evaluating the optical performance across the entire spectral regime of interest as a function of the input beam wavenumber. We display an example emission spectrum of the laser tuned to 1696 cm^{-1}, as shown in Fig. 3a. It is clear that the laser exhibits high S/N with the noise floor at −75 dBm, but in rare cases we measure additional emission at unwanted frequencies, likely due to inadvertent over-driving of the laser. Each of the four laser sub-modules within this system has a spectral tuning range between 200 and 400 cm^{-1}, as can be seen in Fig. 3b, which shows the output emission spectral peaks at different tuning positions. These lasers can be operable in continuous-wave or pulsed modes with repetition rates of 100 kHz up to 2 MHz and duty cycles approximately 5% to 30% depending on the selected configuration, representing pulse widths of ~70 ns. The output emission for a representative IR pulsed laser is shown in Fig. 3c. In order to evaluate noise and bandwidth at each tuned wavenumber, a common way of visualizing the emission across the spectrum is by using a spectrograph, as shown in Fig. 3d. We can also measure the full width half-maximum (FWHM) or the spectral linewidth as acquired and shown in Fig. 3e. The linewidth of each tuned wavenumber can range from 2 cm^{-1} up to almost 4 cm^{-1}, even within a single laser module. As opposed to globar sources, which exhibit negligible differences in spectral irradiance, the performance of semiconductor lasers is often directly affected by manufacturing variance.

The S/N of an imaging system is a crucial figure of merit, which often has a nonlinear dependence as the square root of the magnitude of the signal detected and it can be improved by increasing the input flux or decreasing the noise in both the source and the detector. Although this implies that a high laser output power is typically desired, it has an increased risk of damage to cells or tissues caused by phototoxicity and thermal damage. Output power and noise characterization of the QCL is an essential first step before the optical setup and alignment process. Figure 3f shows the spectral output power for two different laser systems, which exhibit a considerable variation across the entire spectral regime of interest. One way to mitigate the effect of this variability is to either dynamically adjust the sensitivity and range of the detection system accordingly or calibrate the pumping current, pulse rate, or duty cycle of the laser to normalize the total flux incident on the sample. Furthermore, different lasers can also exhibit different levels of pulse-to-pulse variation, which
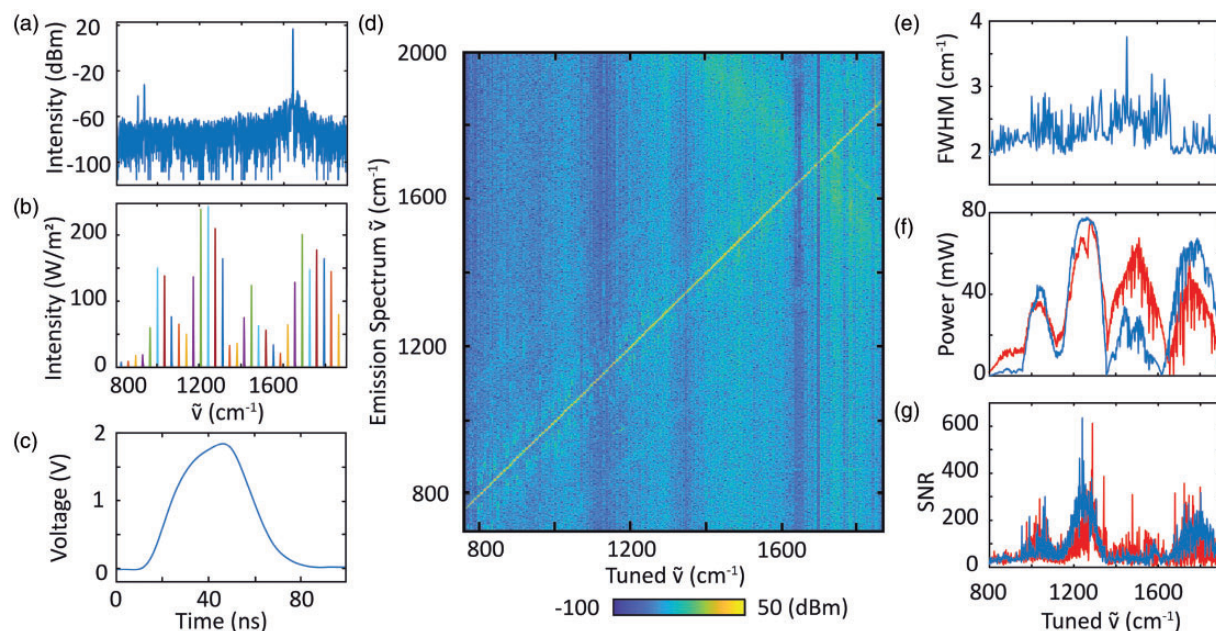
Figure 3. (a) Emission spectrum at 1696 cm^{-1}. (b) Power spectral intensity of the four-chip QCL laser acquired at every 20 cm^{-1}. (c) IR pulse at 913 cm^{-1} wavenumber acquired on the oscilloscope using MCT detector. (d) Emission spectra acquired at 1 cm^{-1} using an FT-IR system for the QCL tuned wavenumber. (e) Spectral linewidth variation of the laser across 770 to 1874 cm^{-1} shows a typical value of 2 cm^{-1}. (f) Average output power of two representative QCLs when pulsed at the repetition rate of 1.3 MHz and 5% duty cycle across the spectral range. (g) S/N ratio of two separate four-chip QCLs as measured across the spectral range.

directly affects the laser output noise and the S/N of the overall system, as shown in Fig. 3g.

Detector

Infrared detector designs can be broadly divided into two major categories depending on the mechanism that is used for converting radiant energy into electric signal. Thermal detectors, including pyroelectric detectors and silicon bolometers, measure the induced temperature change through the pyroelectric effect, or with thermoelectric transducer elements that exhibit the Seebeck effect, respectively.[176]

Photon or quantum detectors operate based on the photoelectric effect and produce free charge carriers that change the electrical characteristic of the responsive element upon incident illumination.[177] Irrespective of the detection mechanism, a few specifications are crucial in the detector choice, namely responsivity, spectral efficiency, response time, and any thermal constraints in terms of the operating temperatures. Although thermal detectors typically exhibit an approximately flat spectral response that is well suited for most applications, they have longer response time, typically in milliseconds, and have lower detectivity, when compared to quantum detectors. Despite these characteristics, many thermal imaging applications do not require extremely high responsivity or frame rates, thus making bolometers that are based on pyroelectric effect ideal for many imaging applications, especially due

to their availability in large formats and their relatively low cost.[177]

The designs of photon detectors broadly fall under photoconductive (PC) and photovoltaic (PV) technologies. Photon detection can be accomplished for both these technologies either using intrinsic semiconductors, without any impurities or extrinsic semiconductors that are doped with controlled impurities. Such detectors that are based on intrinsic semiconductors usually operate at higher temperatures compared to their extrinsic counterparts, exhibit higher quantum efficiencies, with fast response time typically in nanoseconds, and dissipate less power. The most popular intrinsic PV sensor materials are MCT and indium antimonide (InSb). The PV technology with intrinsic photoexcitation consists of the Schottky barriers detector on silicon, platinum silicide, or gallium indium antimonide strain layer superlattices (SLS). SLS are fabricated by intentionally introducing small mismatches between the crystal structures to introduce controlled strain, which theoretically leads to lower dark current compared to existing detector technologies.[178,179] SLS technology shows potential to allow for detector operation at higher temperatures and reduce the necessity of the stringent cooling requirements,[180] but has yet to achieve that in practice. Extrinsic photoexcitation is predominantly based on PC technology and designs often consist of SiGe heterojunctions, impurity band conduction, and solid-state photomultiplier. A novel alternative approach using the III–V hybrid technology is the
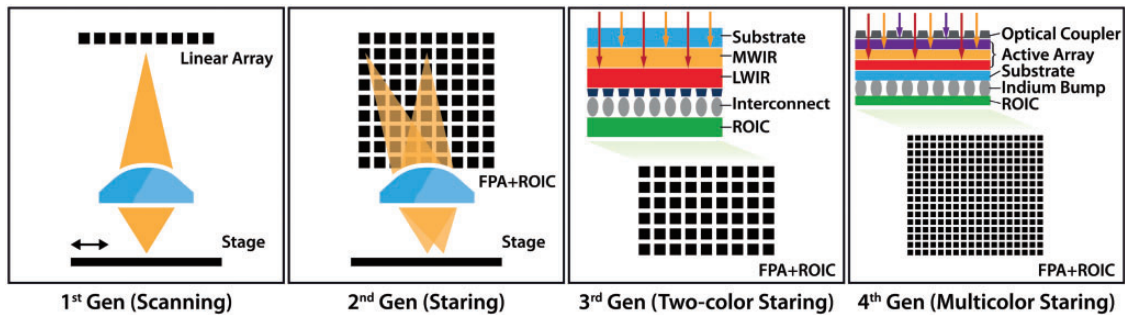
Figure 4. Development of IR detectors and systems technology that can be considered for principal military and civilian applications is shown. Four generation systems spanning, (a) the first-generation scanning systems, (b) second-generation staring systems with integrated system on chip ROIC systems to (c) the third-generation and (d) fourth-generation multispectral large format array systems are as shown.

AlGaAs multiple quantum wells infrared photodetector (QWIP),[181] which also promises next-generation detectors with higher quantum efficiency and operating temperatures. With improved manufacturability, uniformity, and higher yield, these QWIP detectors can be fabricated as large format FPAs at lower cost.[182,183]

Both thermal and photon detectors can be tailored for a specific wavelength regime in the near-infrared between 0.75 and 1.4 μm, shortwave infrared (SWIR) between 1.4 and 3 μm, mid-wavelength infrared (MWIR) between 3 and 8 μm, or in the long-wavelength infrared (LWIR) between 8 and 15 μm. With the atmospheric water window between 5 and 8 μm, instruments are typically purged with dry air to avoid interference from water vapor absorption. Although intrinsic germanium and silicon-based photodiodes were widely used during the 1950s, the low response time and limited spectral response paved the way for development of variable band gap semiconductor alloy-based quantum detectors. Typical materials used for detectors are based on narrow band gap semiconductors, such as InSb, InGaAs, GaAs, or MCT. The fundamental properties of narrow-gap semiconductors include a high optical absorption coefficient, high electron mobility, and low thermal generation rate. The unique capability for band gap engineering to suit the desired spectral range make these hybrid systems ideal for a wide range of IR detectors. The spectral cut-off wavelength for a quantum detector in μm is calculated as $\lambda_c = 1.24/Eg$, where Eg is the band gap energy in eV.

The development of IR detectors and systems was marked by several crucial technological milestones. The first-generation detector designs, shown in Fig. 4a, comprised of single-element or linear photoconductor arrays that were incorporated into FT-IR scanning microscopes. These systems relied on scanning optics and mapped the sample point by point. While the dark noise and amplifier noise are unavoidable barriers for all detectors, these IR detectors were especially affected by thermal and background noise from the ambient environment. Further advancement of sensor materials and microelectronics

spurred the development of second-generation IR detector technologies that were based on photodiodes with integrated detection and readout schemes. This led to the development of large scanning and staring FPAs,[184] shown in Fig. 4b, with individual detector elements configured in a two-dimensional (2D) array. Third-generation systems saw the development of two-color detectors spanning multiple spectral bands, as shown in Fig. 4c.[185] The 2D array configurations enabled the development of IR imaging systems with much higher data throughput and broad wavelength sensitivity. Such arrays were developed as sensor chip assemblies, bonded to readout integrated circuit (ROIC) in order to accumulate the pixel-wise photocurrent, which was routed onto output taps for readout. The fourth-generation IR detector systems (Fig. 4d) promise higher pixel sensitivity, format size, integrated efficient cooling technologies combined with on-chip pixel level processing. Collectively, IR sensor development went through some crucial milestones and design changes since 1970s, ranging from early single-element sensors to large-format monolithic FPAs with integrated on-chip signal processing. A roadmap for IR detector development over the past several decades and across technological generations is summarized in Figs. 4a to 4d.

Single-element detectors were initially characterized by the noise equivalent power (NEP), which is the light intensity that is equivalent to a detector's noise floor, but the need to compare different detector technologies and geometries necessitated the normalization to the square root of the detector area and the electrical bandwidth,[184,186] leading to the concept of specific detectivity. Specific detectivity (D*) for a fixed active area (A), bandwidth (Δf_{BW}), and at a specific optical wavelength is defined as $D^* = \sqrt{A\Delta f_{BW}}/\text{NEP}$ and is commonly expressed in cm·$\sqrt{\text{Hz}}$/W. While D* was well suited for characterizing single-element detector performance, it was insufficient to fully characterize 2D FPA imagers. For example, an LWIR FPA operating at high background noise with background-limited performance (BLIP) S/N can have a D* that is numerically lower

than an SWIR detector having poor S/N relative to the theoretical limit.[184] Thus, the development of FPA technology involved new considerations, including multiple trade-offs between several key parameters, where, e.g., the choice of format size and pixel pitch of the ROIC can greatly affect the sensitivity and noise characteristics of the instrument.[183,187,188] FPAs are typically characterized by their noise equivalent temperature difference ($NE\Delta T$), representing the minimum detectable temperature difference matching the camera's internal noise, and defined as[189]

$$NE\Delta T = \left(\tau C \eta_{\text{BLIP}} \sqrt{N_\omega}\right)^{-1} \qquad (1)$$

and is a function of the optics transmission spectrum (τ), thermal contrast (C), the ratio of photon noise to the composite FPA noise (ηBLIP), and the number of photogenerated carriers (N_ω). The carriers can be represented as $N_\omega = \eta A_d t_{int} Q_B$, proportional to the integration time (t_{int}) and the photon flux density (Q_B) on the effective detector area (A). As $NE\Delta T$ is inversely proportional to the square root of the integrated charge, we see an improved performance as we increase the well depth of the sensor. The sensor noise described by $NE\Delta T$ is directly related to the operating temperature for various sensor technologies. Two crucial interlinked parameters affect the final acquisition time of the detector and hence the FPA performance, namely the single-pixel readout rate, which is the time required to digitize the signal at each pixel, as well as the frame transfer rate, which is the total readout time for an entire 2D array of pixels. The charge handling capacity of the readout, the trade-offs between integration time and the frame time, and dark current of the sensitive material are all major issues limiting the performance of IR FPAs.[182]

Focal plane array development in the mid-IR has not kept pace with visible array detectors for obvious reasons of commercial volume and ease of fabrication. The largest IR FPAs were often used for ground-based astronomical telescopes, which include up to a 147-megapixel camera by Teledyne Imaging Sensors that comprises of 35 individual arrays, each with 2048×2048 pixels.[190] However, these were typically one-off productions that were cost prohibitive for applications outside of astronomy or defense. FPAs used for spectroscopic microscopy were typically much smaller with 128×128 pixels. However, advances in detector technology, readouts, digital electronics, miniaturization, and reduced costs of packaging all point to a ripening of conditions to accelerate the development of better performing IR array detectors and systems. Greater availability and selection of size and characteristics will likely spur new innovations and their use for a segment of IR imaging. Furthermore, uncooled alternatives are also showing up in the market. The key trade-off with respect to uncooled thermal imaging systems is between sensitivity

and response time. Presently, vanadium oxides microbolometer array is the most prevalent technology, being inexpensive and operable at room temperature. Recent advances in the cooling technologies and multi-band detectors have introduced MEMS-based tunable IR detectors with voltage-tunable multiband IR FPAs. Furthermore, vertically integrated sensor array hybrid technology with 2D arrays of indium-bump interconnects to the silicon readout is a potential solution to significantly increase both, the charge storage capacity and the dynamic range.[191,192] Significant efforts in visible detector readout circuits and improved fabrication has led to larger formats and reduced fabrication costs. It is likely that these advances will enable similar gains in IR analytical instruments.

Currently, thermoelectrically cooled MCT detectors with multiple stages are the most widely used variable band gap semiconductor alloys for IR photodetectors in scanning instruments.[183] With band gap energy values as low as 0.07 eV, high-performance quantum detectors can be tailored with spectral range spanning up to 18 μm. Specifically, single-element MCT detectors offer good spectral characteristics with $D^* \geq 2 \times 10^9$ across the entire spectral range from 1 to 12 μm and are ideal for fast readout rates and low cost. These sensors can be optically immersed through monolithic integration with high refractive index microlenses resulting in an increase in effective optical area of the detector by n or n^2 for hemispherical and hyperhemispherical geometries, respectively, where n is the refractive index of the lens material.[193] For a hyperhemispherical GaAs microlens, this can increase the effective detector area by almost elevenfold, which improves D^* by one order of magnitude and electrical capacitance by a factor of two orders of magnitude compared to conventional detectors with equal optical area. The continued development of higher intensity sources, better electronics and faster computing will likely see performance improvement of these detectors to match needs in new applications.

Optics

An optimal integration of the source and detector assemblies within a microscopy system is accomplished by selecting suitable optics that efficiently relay light from the source, through the sample, and to the detector. While a QCL can be adapted to existing IR microscopes with moderate changes, the use of refractive optics requires a comprehensive redesign as we approach diffraction-limited performance. However, the dominant challenge in the design and fabrication of novel systems is the limited availability of optics that are both well corrected over a reasonable FOV and have a flat transmission curve over a broad wavelength range. The first instances of QCL widefield designs as described in Figs. 1c and 1d used completely reflective relay optics with stock Schwarzschild objectives,
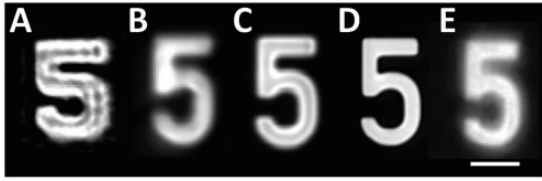
Figure 5. Absorbance images of SU-8 photoresist patterned as a USAF 1951 resolution test target with the Group 5 numeric shown. A progression of DFIR improvements in resolution over the recent years include (a) Widefield[132] and (b–d) point-scanning[135,145,195] design configurations respectively, when compared to (e) a comparable feature acquired using HD FT-IR. The scale bar is 40 μm.

which considerably degraded image quality due to the presence of the central obscuration. For comparison, a widefield design with refractive optics described in Fig. 1b, using off-the-shelf spherical mirrors and refractive singlet objective lens, showed significant improvements in performance. The improvements in resolution of subsequent generations of DFIR imaging systems, due to better understanding of these design principles over the years, is shown in Figs. 5a to 5e. However, these simple stock optics with long focal lengths and weak focusing power are not effective as the primary focusing objective for microscopy. Furthermore, optics with basic curved surfaces inevitably introduce spherical aberration in the imaging system, which can only be corrected by using computationally intensive post-processing techniques.

Selecting refractive optics is the first step toward designing an IR microscope. The effective focal length, the working distance, the NA, the lens magnification, and the transmission efficiency across the spectral range are a few vital specifications that need to be considered. The signal intensity incident or acquired is directly related to the square of the lens NA, which is inversely proportional to the square of the lateral magnification. High NA objectives are often more difficult to correct for aberrations, resulting in higher complexity and cost, but they also collect more light and produce an image that is brighter with higher resolution. Finite conjugate lens systems are relatively simple in design, requiring only a few components compared to an infinity-corrected design consisting of both a compound objective and a multi-element tube lens. With the migration to infinity-corrected design, a new set of criteria was necessary to properly correct for optical aberrations. Seidel extended the Gaussian theory of rotationally symmetric lens systems to include monochromatic ray aberrations, which occur due to the deviation of predicted performance of an imaging system from paraxial optics, up to the third order.[194] Most of the current software optimizers correct for the prime third-order aberrations, such as spherical aberration, coma, astigmatism, curvature of the field, and distortion, across the FOV while controlling

sensitivity to manufacturing tolerances. Given the advancements, this area is opportune for innovations to provide imaging capabilities in the IR that are currently existing in visible and near-IR regimes. The system can be usually optimized over the desired wavelength range as well as different fields, either with respect to the image side or object side. Usually, wider the operable spectral range and target FOV, the more the complexity in the design to account for any deviations. The complexity typically manifests in terms of the increased number of surfaces, surface geometry types, such as spherical or aspheric, and different selection of materials. Regardless, the field of IR microscopy is poised to move forward from a decade long exclusive focus on all-reflective optics to better understanding, developing, and using refractive optics.

Aberration correction is the primary driver of the lens assembly to be used. Achromatic doublets, using materials of dissimilar refractive index and dispersion characteristics in combination, are prevalent for aberration corrections. The selection of component materials and their optical properties directly affect the ability of the complete lens assembly to resolve images across the design FOV and wavelength range. Furthermore, parameters including cost, weight, thermal variation of refractive index, and means of manufacturing must also be considered during the material selection process. In comparison to the large variety of glasses usually used in the design of visible microscopy components, the number of material choices in the IR regime is significantly reduced. Crystalline materials such as Ge, Si, zinc selenide, barium fluoride, calcium fluoride, GaAs, zinc sulfide, and thallium bromoiodide can be typically fabricated by conventional grinding and polishing or single-point diamond turning. Amorphous chalcogenide glasses that are IR transparent are also available and, in some cases, can also be fabricated cheaply in bulk through a molding process. Many of these materials have a very high refractive index, which necessitates the use of multilayered anti-reflective coatings to achieve broadband performance. All of these materials exhibit chromatic dispersion or a wavelength-dependent refractive index, which is usually quantified by the Abbe number (V_d). The Abbe number is typically measured in the visible regime using three wavelengths 587.6 nm (He d-line), 656.3 nm (H_2 C-line), and 486.1 nm (H_2 F-line), as an index difference between the extreme ends of the spectral region

$$V_d = \frac{n_d - 1}{n_F - n_C} \tag{2}$$

Dispersion is defined at the short and long wavelengths of interest in the IR, typically at an average wavelength for the mid-wave (3–5 μm) and long-wave (8–12 μm) regions.[177] A higher Abbe number indicates a greater change in the focal length and a lower degree of chromatic dispersion. Another measure for characterizing the optical

properties of the IR glasses is the partial dispersion that is calculated as

$$P_d = \frac{n_F - n_d}{n_F - n_C} \tag{3}$$

The Abbe diagram for some common IR compatible optical glasses and their partial dispersion is shown in Figs. 6a and 6b, respectively. The design process will often begin by selecting fictitious materials with refractive index and Abbe number within the bounds defined by this diagram. Using an iterative strategy, the design can be optimized to a set of real materials that meet the required refractive index, transmission, and other optical parameters. By balancing performance requirements, the design can be further optimized based on criteria such as effective focal length and system resolution. For instance, variation in the spot diameter with respect to the objective incident angle and the wavelength, for an objective comprising of a certain Black Diamond-2 (BD-2) glass, can be simulated, as shown in Fig. 6c. Using tolerance analyses, the variations in lens parameters can be controlled, while the addition of adjustable compensators can be used to optimize the design in a way that minimizes manufacturing complexity while satisfying performance goals. Stringent tolerance requirements typically result in substantially higher manufacturing costs. A well-designed system is less sensitive to manufacturing variations and promises a higher cumulative probability of achieving the predicted performance. In other words, while the optimizer can predict the likelihood of successful construction, ultimately the as-built system must be tested and evaluated against its originally simulated performance.

This gap between modeling, rapid hardware prototyping, and manufacturing capacity is a key stumbling block for the continued development of IR imaging. The manufacturing complexity of compound lens assemblies, their high cost due to limited volumes, and difficulty in quality assessment make widespread availability difficult. Important ideas in optical design, such as free-from optics, molded lenses, and diffractive optics, have been slow to be adopted or non-existent in use for IR microscopy. This large reservoir of advances can be used to generate innovative tools that are accessible to many instrument designers and users. However, a cycle of applications, design innovations, prototyping, and adoption for better applications will need to be initiated. At this time, there is growing evidence that new components and new designs are catalyzing this cycle. An important aid to progress has been the recent focus on theoretical frameworks to understand IR imaging systems that allow a systematic analysis of new ideas, and performance assessment of systems.

Performance Assessment

A theoretical understanding of light propagation through an optical system and resulting image formation is necessary for a rational design of advanced instruments.[4] With coherent illumination of the object and a linear-time invariant assumption, a DFIR imaging system is linear in the complex amplitude field. An example DFIR imaging system can be analytically described using Fourier optics[196] as a relation between the optical field or the irradiance pattern of an object at the image and object planes, and can be mathematically described by

$$U_i(u, v) = U_O(u, v) \otimes h(u, v)$$
$$h(u, v) \xrightarrow{\mathcal{F}} H(\rho_x, \rho_y) \tag{4}$$
$$G_i(\rho_x, \rho_y) = G_O(\rho_x, \rho_y)H(\rho_x, \rho_y)$$

where the real image, $U_i(u, v)$, is the convolution between the point spread function (PSF) of the system, $h(u, v)$, and the original object, $U_O(u, v)$, and u and v represent position co-ordinates in the spatial domain in the image plane. The normalized pupil function is denoted as $P(x, y)$, where x and y are the spatial co-ordinates in the principal plane of the imaging system. The equivalent Fourier domain model is
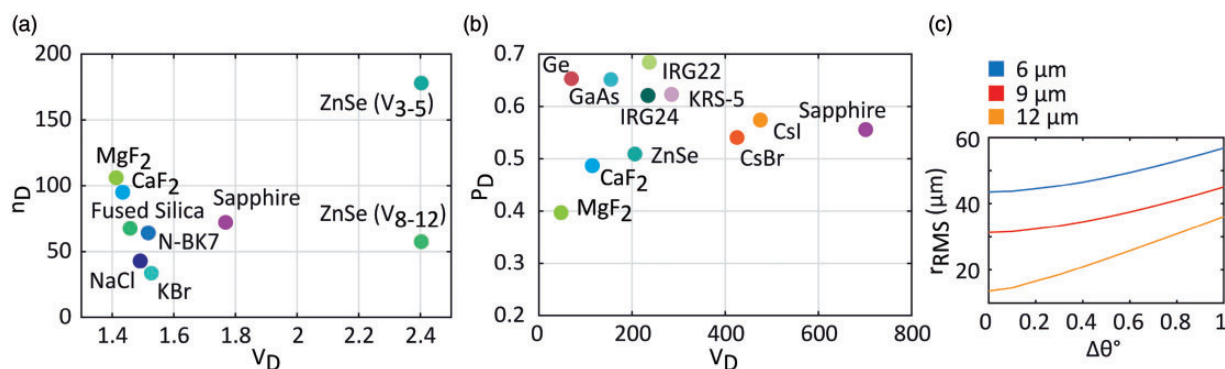
Figure 6. (a) Abbe diagram for different IR materials as a function of the Abbe number. (b) Partial dispersion variation for different IR materials as a function of the Abbe number. (c) Variation in the RMS error at the spot diameter with respect to the incident angle on the objective as a function of the wavelength. Simulation was performed using CODE V.

simply a multiplication of $G_O(\rho_x, \rho_y)$ and $H(\rho_x, \rho_y)$, the 2D FT of the PSF, also known as the amplitude transfer function of the imaging system; ρ_x and ρ_y are normalized spatial frequencies in the u and v directions, respectively. Assuming a diffraction-limited coherent imaging system, the image intensity or irradiance detected at position (u, v) is simply the time-averaged value of the square of the image amplitude field

$$I_i(u, v) = \langle |U_i(u, v)|^2 \rangle \tag{5}$$

For a conventional DFIR microscope,[197,198] the intensity at the image plane is given by $I_{conv}(u, v)$

$$I_{conv}(u, v) = \left| \int \int h(u, v) U_O\left(x - \frac{u}{M}, y - \frac{v}{M}\right) du\, dv \right|^2 \tag{6}$$

Extending this formulation, a confocal DFIR microscope with a given pupil function can be described by the standard mathematical model given by the intensity in the detection plane at position (u, v) by $_{conf}(u, v)$ as

$$I_{conf}(u, v) = \left| \int \int h_1(u, v) h_2(u, v) U_O\left(x - \frac{u}{M}, y - \frac{v}{M}\right) du\, dv \right|^4 \tag{7}$$

in which h_1 and h_2 are the amplitude PSFs of the illumination and imaging lenses, also known as the condenser and objective, respectively, while M represents the total magnification of the system. For an imaging system in epi-illumination configuration where a single-lens assembly performs both the illumination and imaging functions, $h_1(u, v) = h_2(u, v)$. For a circular pupil function $P(x, y)$

$$P(x, y) = circ\left(\frac{\sqrt{x^2 + y^2}}{D/2}\right) \tag{8}$$

the corresponding coherent transfer function is given as

$$H(\rho_x, \rho_y) = circ\left(\frac{\sqrt{\rho_x^2 + \rho_y^2}}{\rho_c}\right) \tag{9}$$

where $\rho_c = D/\lambda f$ is the spatial cut-off frequency of a perfectly coherent imaging system, f is the focal length, and D is the effective aperture or the entrance pupil diameter. The understanding of image formation and data recording in the IR domain is still in its infancy. We anticipate that there is significant upside to understanding image formation as a function of spatial structure, (dynamic) properties of constituent materials, and the effects of different optical configurations of the recorded data. Mathematical modeling is an area of investigation that has direct benefits to the design of the next generation of instruments, while also presenting new opportunities to extend the practice of applied spectroscopy beyond structure–property relationships at the molecular level. As instrumental configurations diversify, we anticipate that the fidelity of spatial and spectral data will be more rigorously understood in terms of instrument design and limitations of the methods of recording data while opening new avenues that could enable mapping of molecular dimensions in an imaging format, for example in understanding the spatial distribution of molecular chirality.[175]

Optical Resolution and Contrast

Optical resolution for an imaging system is defined as the minimum resolvable distance between two-point objects in the sample plane. Understanding the mathematical basis of image formation is an essential step for comparing the theoretical limits of lateral resolution of a conventional and a confocal microscope. Assuming a circularly symmetric pupil and a point object, the intensity in lateral and axial directions for a conventional widefield system is given as

$$I_{conv}(0, v) \propto \left(2\frac{J_1(v)}{v}\right)^2, I_{conv}(u, 0) \propto \left(\frac{\sin(u/4)}{u/4}\right)^2 \tag{10}$$

where J_1 is the first-order Bessel function. The normalized optical co-ordinates in the radial and axial directions are, respectively, given by u and v as $u = 8\pi\tilde{v}zn\sin^2(\alpha/2)$ and $v = 2\pi\tilde{v}rn\sin(\alpha)$, where $\tilde{v} = 1/\lambda$, specifies the linear wavenumber, λ is the wavelength, n is the refractive index of the immersion medium, α is the angular aperture, and $n\sin(\alpha)$ denotes the NA or the resolving capability of any lens system. Note that u and v represent the actual axial distance, z, and radial distance, r. The FWHM can be estimated in both lateral and axial directions by evaluating the value of $u_{FWHM} = 1.61$ and $v_{FWHM} = 1.16$ at which the intensity is equal to half of the maximum value at $u = 0$ and $v = 0$, respectively. Theoretically, this can be approximated by

$$\Delta r_{conv} = 0.51\frac{\lambda}{NA_{obj}}, \Delta z_{conv} = 0.89\frac{\lambda}{n - \sqrt{n^2 - NA_{obj}^2}} \tag{11}$$

where Δr_{conf} and Δz_{conf} are the lateral and axial resolutions for the confocal configuration, respectively. The lateral optical resolution of all microscopes is primarily determined by the magnification and the NA of the objective lens, NA_{obj}, hence they are often prominently marked with these specifications as, e.g., "20 × /0.5".

The intensity in lateral and axial directions for a confocal system is given as follows

$$I_{conf}(0, v) \propto \left(2\frac{J_1(v)}{v}\right)^4, I_{conf}(u, 0) \propto \left(\frac{\sin(u/4)}{u/4}\right)^4 \tag{12}$$

The FWHM can be estimated in both lateral and axial directions by evaluating the value of $u_{FWHM} = 5.57$ and $v_{FWHM} = 4.01$ at which the intensity is equal to half of the maximum value at $u = 0$ and $v = 0$, respectively. In a confocal system, we see a theoretical improvement in optical resolution by factor of $\sqrt{2}$ compared to traditional microscopy systems in both the axial and radial directions for the same value of λ and NA_{obj}. It can be approximated as

$$\Delta r_{conf} = 0.37 \frac{\lambda}{NA_{obj}}, \Delta z_{conf} = 0.64 \frac{\lambda}{n - \sqrt{n^2 - NA_{obj}^2}}$$

(13)

where Δr_{conf} and Δz_{conf} are the lateral and axial resolutions for the confocal configuration, respectively. For a confocal microscope in epi-illumination configuration, the objective lens performs both illumination and imaging functions. The effective PSF of the confocal system, described in Eq. 7, is significantly smaller compared to the conventional system described in Eq. 6, since it is product of the individual PSFs of the condenser and the objective lenses.[199,200] Figures 7a and 7b compare the lateral and the axial resolutions, respectively, of the conventional and confocal microscopy systems. Approximately, the axial resolution can be estimated as twice the lateral resolution of the imaging system.

The theoretical basis for understanding optical resolution of an imaging system can be described in Eqs. 11 and 13. The formulation is similar to the definition of resolution for optical microscopy in the context of the diffraction limit as estimated by the Abbe[201] and Rayleigh[202] criteria.

In practice, image contrast and resolution are inseparable parameters that can be principally used for characterizing the spatial resolution of an image.[203] It is important to remember that contrast in IR arises from absorption and is not constant across the spectrum. This affords an opportunity to extend the resolving capabilities of IR microscopy beyond the optical limits that assume a flat or integrated spectral bandwidth.[204–207] Akin to time course measurements for superresolution fluorescence microscopy,[208,209]

Figure 7. Variation of (a) radial resolution and (b) axial resolution with the incident wavelength for conventional and confocal microscope for $NA_{obj} = 0.71$.

spectral data offer opportunities for superresolution,[210] but these have not been practically realized yet.

The modulation transfer function (MTF) is the measure of a linear, space invariant imaging system's spatial frequency response. Although traditionally, MTF has been defined for incoherent imaging systems as the modulus of the auto-correlation of the pupil function, $H(\rho_x, \rho_y)$, most optical design tools specify MTF as a metric for optimization of the optical systems with coherent sources. Hence, even though the amplitude coherent transfer function is the correct metric for optical performance, MTF is still defined and measured for coherent imaging systems. Especially with diffraction-limited resolution, it is a good assumption that helps us in assessing the performance across various degrees of source coherence. Finally, the effects of both spatial and temporal coherence on the detected irradiance is an area that needs further investigation.[211] Note that the complete system MTF of an imaging system is the product of the MTF of all its individual components, including the detector and the optics. Mathematically, the MTF of an ideal aberration-free incoherent imaging system[211] with a uniformly illuminated circular pupil equals

$$MTF = \frac{2}{\pi}(\phi - \cos\phi\sin\phi)$$

(14)

where $\cos\phi = \rho/\rho_c$, and $\rho_c = 2D/\lambda f$ is the spatial cut-off frequency of an incoherent imaging system and $\rho = \sqrt{\rho_x^2 + \rho_y^2}$. The detector MTF[212] is given as

$$MTF_d = \{sinc(d_x\rho_x)sinc(d_y\rho_y)$$

(15)

where d_x and d_y are the photosensitive detector sizes. Thus, at any given wavelength, λ, the MTF is determined by the limits set by the detector size and the system aperture. The two important limiting regions of operation are when the MTF is optics-limited, and the other extreme end is when it is detector-limited. For instance, in the detector-limited region, changing the f number (f/D) does not significantly affect the system resolution. Alternatively, in the optics-limited region, changing the detector size has negligible effect on the system resolution. The detector-limited and the optics-limited regions are as shown in Fig. 8 between $0.41 < f\lambda/D < 1$.

The system MTF can be experimentally determined by a variety of different methods that have been developed over the past decades. The contrast in a periodic grating pattern consisting of alternating transparent and opaque bars of equal width is a standard method to quantify the resolving power of the imaging system. The contrast of the image is plotted against the spatial frequency, measured in line pairs per millimeter (lp/mm) of the features on the test target. One such example is the USAF 1951 resolution test target shown in Figs. 9a and 9b consisting of groups of horizontal and vertical bars organized in elements of progressively
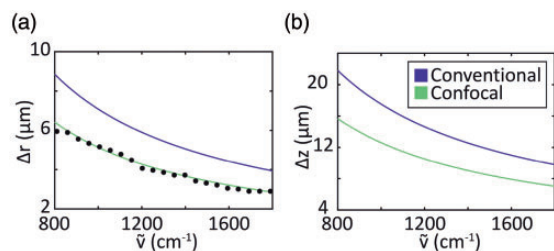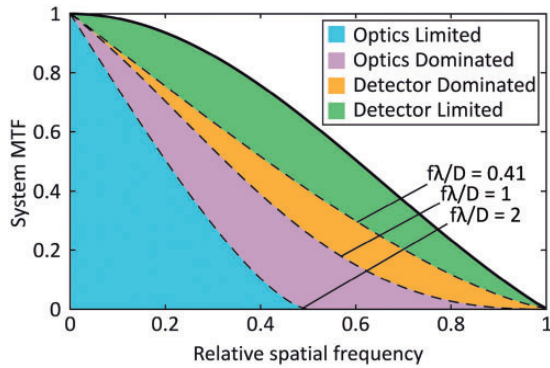
Figure 8. Simulated system modulation transfer function (MTF) and detector MTF curves illustrating the different regions with the design space for various $f\lambda/D$ conditions. Spatial frequencies are normalized to the detector cut-off frequency. Reproduced with permission from Rogalski.[179] Copyright 2017 SPIE.
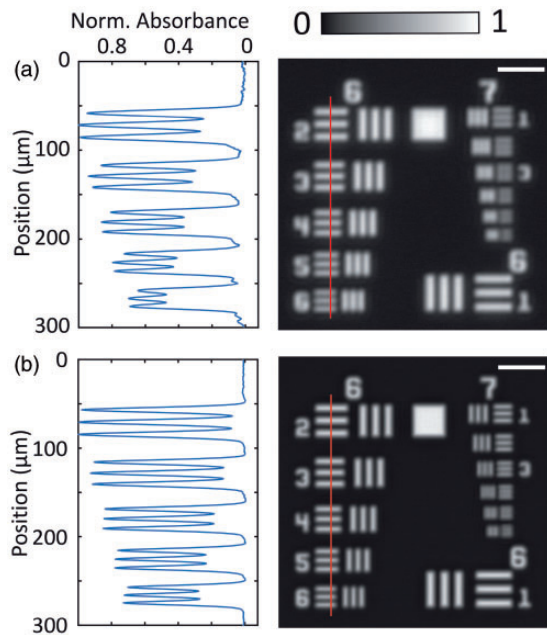

Figure 9. Absorbance image of the USAF 1951 chrome on glass negative resolution test target acquired at (a) 1000 cm^{-1} to determine the spatial frequency resolution and (b) 1600 cm^{-1} of a representative DFIR system. Corresponding vertical line profiles of Group 6. All scale bars are 50 µm.

decreasing size. By determining the element in the group where the bars are no longer resolvable, we can specify the resolution of the imaging system in lp/mm as $2^{\text{Group \# + (Element \# − 1)/6}}$. Thus, in Fig. 9a, since the Group 7 Element 2 is resolvable, the system resolution is estimated to be 143.7 lp/mm or 3.5 µm. Similarly, in Fig. 9b, since the Group 7 Element 5 is resolvable, the system resolution is estimated to be 203.2 lp/mm or 2.5 µm. The target was imaged at two different wavenumbers, 1000 cm^{-1} and

1600 cm^{-1}, to demonstrate the effect of the wavenumber of the incident IR light on the contrast and image quality. As expected, the resolution varies greatly across the bandwidth and improves with increasing wavenumber when pixel size and optical setup are constant. Furthermore, we can plot line profiles across the elements of Group 6.

The slanted-edge method[213,214] is one of the fastest methods to approximate the spatial frequency resolution of an imaging system by imaging an edge with a sharp transition that divides the image area into transparent and opaque regions. Mathematically, this is equivalent to applying the Fourier-slice theorem to the projection of the system's PSF obtaining a radial slice through the two-dimensional MTF of the two-dimensional PSF. The MTF can be computed by taking the magnitude (modulus) of the FT of the system's impulse response or the PSF. As shown in Fig. 10a, the pixel intensities at the slanted edge are projected orthogonally and super-sampled with sub-pixel resolution, which provides the edge spread function (ESF). The derivative of measured ESF is the system's line spread function (LSF), and the modulus of the FFT of the LSF is equal to the MTF. The LSF is the line integral of the PSF, where the FWHM is indicative of the imaging system's resolution for a specific wavenumber. The sampling frequency for the ESF should be greater than the Nyquist frequency of the imaging system, which is defined as the highest sinusoidal frequency that can be represented uniquely. Although the slanted-edge method is not based on any assumptions of rotational symmetry for the 2D PSF or the estimated MTF, it does require a high-fidelity representation of the ESF. For accurate estimation of the MTF for a system, the target slanted edge should be slightly misaligned, typically between 1° and 5° with respect to the sensing plane or the pixel grid. The MTF of a system varies across the focal plane, and a test chart with a grid of rectangles covering the entire FOV can also be used.[215] But the accuracy of the MTF estimates is highly dependent on the acquired image edge contrast, the noise levels (S/N) and the edge orientation angle with respect to the horizontal and vertical directions. For systems showing asymmetrical defects, the sagittal and meridional MTFs show a considerable difference and they can be separately estimated instantaneously[214–216] using commercial targets. By capturing edges at consecutive different slant angles, this method can also be extended to reconstruct an approximate 2D MTF and by applying the inverse Radon transform,[217] the full 2D PSF.[218–220] The estimated resolution of a representative system with the slanted-edge method shows the contrast variation with respect to the wavenumber in Fig. 10b.

When characterizing imaging systems that operate over wide spectral ranges, especially in the IR, and hence have a wide variation in resolving power, the concept of system resolution is difficult to estimate. The definition of lateral resolution for a broad hyperspectral system should be,
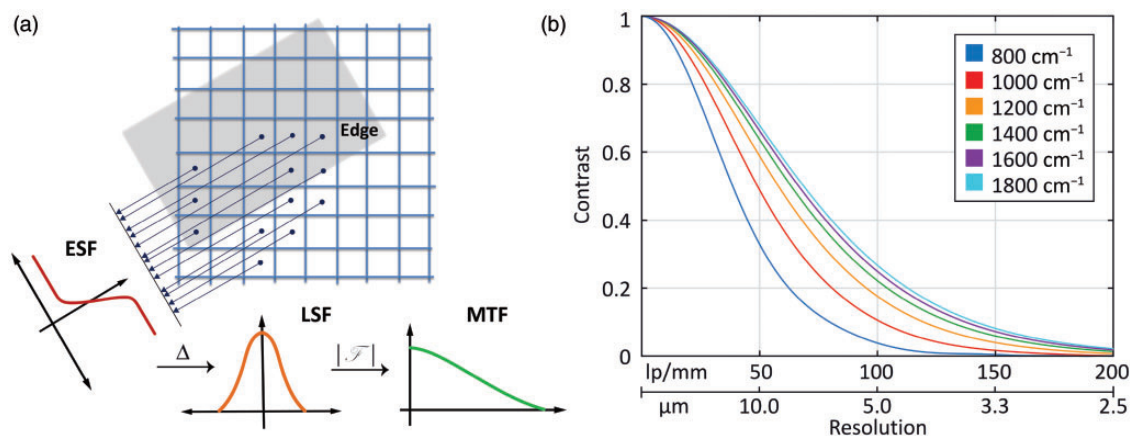
Figure 10. (a) An image of a slanted-edge acquired by a DFIR system is projected orthogonally to generate a super-sampled edge intensity profile, known as the ESF. The derivative of the ESF is used to compute the LSF. The MTF of the system is derived by taking the modulus of the Fourier transform of the LSF. (b) MTF of the DFIR system as a function of wavenumber with an estimated resolution of 3.5 μm at 800 cm^{-1}.

thus, invoked from a decision theory perspective.[221,222] It combines spectral and spatial information to surpass the classical diffraction barrier limit as posed in the IR regime by providing sub-micron information that is below the wavelength of the incident illumination. However, while comparing the resolution of a hyperspectral imaging system with a traditional visible imager, the problem should be formulated from the perspective of the maximum information capacity[223] that is transferable by the imaging system. We do not recommend the continued use of optical resolution as a figure of merit for IR imaging as it does not capture the molecular dependence of the optical response, the effect of the wide bandwidth and effect of the contrast within the image. The idea of spatial resolution is central to application of an imaging system to specific problems as well as to ideas of performance assessment. However, it is now clear that a naive adoption of optical microscopy performance parameters to IR microscopy cannot capture the full potential of the design of IR microscopes. Specifically in IR, the spectral bandwidth has a direct effect on the acquisition times and the quality of acquired data. Hence, we anticipate that efforts into improving spatial imaging capability in the IR region will become even more active and will involve novel optical designs, consideration of spectral separability as a computationally inherent parameter to the analysis of chemical images and actual performance of the imaging system.

Aberrations

Real-world optics typically deviate from the theoretical design performance. As-built performance of the lens system can be better understood by studying the deviations from the ideal design in terms of aberrations. Often, the real PSF $\tilde{h}(u, v)$ or its FT, i.e., the pupil function, $\tilde{H}(\rho_x, \rho_y)$ is used in Eq. 4 to describe the degradation of the image in a physical system with inherent aberrations. Aberrations reduce the imaging system performance through the deformation of the transfer function in both spatial and frequency domains. The most common primary third-order optical aberrations are spherical, coma, astigmatism, Petzval field curvature, and distortion.[224]

Spherical aberration is inherent in simple lenses with spherical surfaces and results in a divergence of focal distances between the marginal rays and the paraxial rays. Aspheric lenses are corrected for this behavior, which results in a diffraction-limited on-axis spot size, albeit with increased manufacturing complexity and cost. When the incident light is off-axis from the principal optical axis, comatic aberrations are apparent, resulting in a characteristic comet-like blur, and this is often indicative of a misalignment in the optical system as can be seen in Figs. 11b to 11c. Most imaging systems are manufactured to be rotationally symmetric, but deviations due to misalignment or manufacturing errors can result in asymmetric focal planes between the sagittal (radial) and tangential rays. Further, lens systems contain multiple elements to correct for field curvature, where the focal plane follows a curved surface. Most converging lenses exhibit an out-of-focus blur toward the edge of the image plane, when the lens is sharply focused on axis, which typically results from an inward field curvature. As described previously, aberrations can be optimized by controlling the design parameters, including the base radii of curvature, departure from the best-fit sphere, lens thickness, geometrical positioning of element, and finally, material selection according to transmissivity, refractive index, and dispersion. In the optical design process, it is also important to consider the specific system requirements and understand the balancing of different aberrations in order to achieve a design that meets manufacturability, cost, and other form-factor restrictions. At times, it is often necessary for a designer to trade-off, for
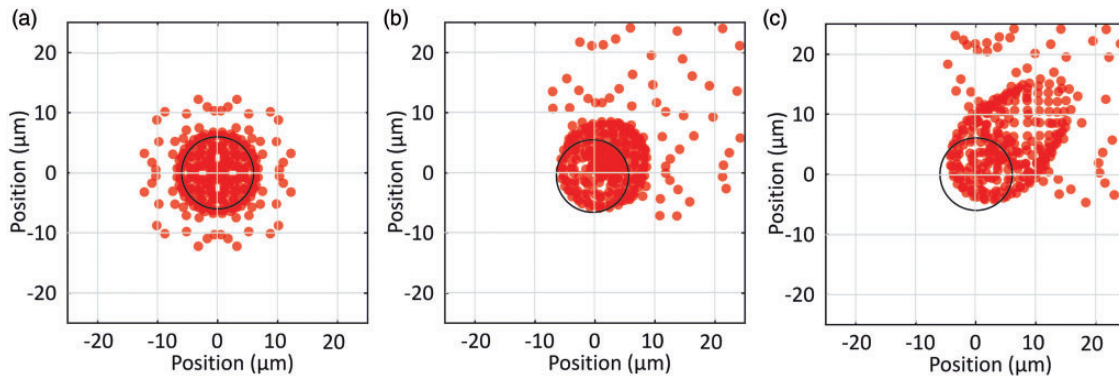
Figure 11. Spot diagram for the 0.71 NA objective at the reference wavelength of 6 μm at an objective incident beam angle of (a) 0°, (b) 5°, and (c) 10°. The image plane is centered at the chief ray and all displacements are listed relative to the chief ray at the reference wavelength for each field. The diffraction-limited spot size (Airy disk) is shown with diameter equal to 2.44 $f\lambda/D$, in which f is the focal length and D is the effective aperture of the lens. Simulation was performed using CODE V.

instance, FOV, for improved resolution. Most notably, in one special lens type, the fish-eye lens, the design achieves extremely wide FOV in exchange for high distortion that is later corrected computationally during post-processing.[225] Another significant aberration, distortion, is a class of optical aberrations in an imaging system that can be measured as the deviation from the rectilinear projection. For the most common types of regular geometric distortions, such as pincushion or barrel, since the information is instead remapped onto a non-uniform grid, post-processing software is widely used for rectifying the distorted image.[226,227] Non-optical-based distortions can also arise in stage-scanning modalities, when the true stage position does not match the target position at a precise time, because of mechanical uncertainties such as drift, instability, or fly-back.[228,229]

Finally, in hyperspectral imaging systems that operate over a wide spectral range, some aberrations reflect a large variation in the imaging performance of the system. Hence, it is important to characterize the system aberrations as a function of wavenumber. A commonly encountered aberration is chromatic dispersion, which results in variation of the system focal point with respect to the incident wavenumber. During spectral scanning, this aberration necessitates a mechanical correction in the working distance of the objective lens from the sample. With discrete frequencies that are acquired sequentially, DFIR systems offer an unparalleled advantage by simplifying the optical design without the need for a high-end achromatic system. As shown in Fig. 12a, the chromatic focal shift for an example 0.72 NA lens is simulated using CODE V for a design wavelength of 7.8 μm = 1282 cm^{-1}. It allows for large rapid changes in the wavenumber, as the autofocus algorithm only needs to perform a small range optimization over a narrowed search space after each tuning command. The simulated case is compared to the experimentally determined focal position via an autofocus algorithm across the system's tunable spectral range from 800 to 1800 cm^{-1}. The deviation that is seen in the true best
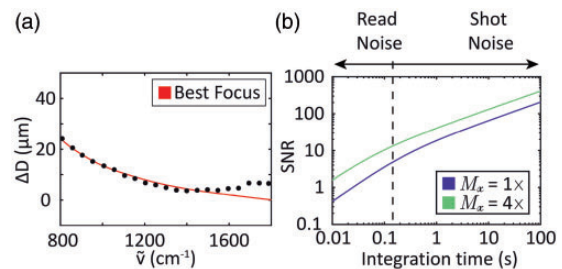
Figure 12. (a) Chromatic focal shift acquired for 0.72 NA BD-2 lens simulated using CODE V for design wavelength of 7.8 μm = 1282 cm^{-1} for best focus case and compared to the acquired data for the spectral range 800–1800 cm^{-1}. (b) Variation of S/N with respect to integration time shows a nonlinear relation, dominated by read noise in low-S/N regime and shot noise in a high S/N regime for two different binning cases, $M_x = 1\times$ and $M_x = 4\times$.

focus from the simulated can be ascribed to a larger angular divergence of the output of the laser chip covering 1600–1800 cm^{-1}. While we have summarized some of the major considerations and factors underlying optical image quality in IR microscopes in this section, understanding the effect of aberrations and their detailed study is likely to be an emerging topic for IR microscope design as the diversity of lenses increases. We anticipate that these will, in turn, revolutionize DFIR technology with the availability of new hardware, software, or control strategies to improve spatial image quality.

Signal-to-Noise Ratio

Noise in an analytical imaging system affects its ability to detect a particular substance during a specific measurement. The ratio of the power of a signal to the power of the noise is often defined as the S/N, which is a compact representation of the information capacity of any imaging

system. Statistically, for an optical signal intensity, S/N is defined as the ratio of mean to standard deviation of the measurement, i.e., S/N = μ/σ, where the expected value of signal is μ and the standard deviation in the signal is σ. While a modified version of the PSF $\tilde{h}(u, v)$ is sufficient to describe the transfer characteristics of a real imaging systems with inherent aberrations, some noise sources are coupled into the process of image generation, $\tilde{U}_O(u, v)$, and hence will be acted upon by the transfer function, $\tilde{h}(u,v)$, while all other spatially variant additive noise sources are explicitly represented by the term $n(u, v)$. Thus, the expression for $U_i(u, v)$ is modified as

$$U_i(u, v) = \tilde{U}_o(u, v) \otimes \tilde{h}(u, v) + n(u, v) \quad (16)$$

Noise contributions can arise at a number of stages throughout the imaging system. For instance, at the illumination stage, the laser pulse-to-pulse fluctuations result in a dominant temporal contribution, whereas any contributions at the scanning and detection stages are spatial. An inherent noise specific to coherent sources is the speckle pattern, which can be simulated in a coherent imaging system described in Eq. 4 by applying a random complex exponential phase term to the object field, i.e., $\tilde{U}_O(u, v) = U_O(u, v)e^{2\pi j\theta}$, where $\theta \sim \mathcal{N}(\mu = 0, \sigma^2)$.

Infrared imaging systems are intrinsically limited by the detector noise floor and sensitivity.[230,231] Previous work[48,71,230,232] has explicitly evaluated the S/N for IR systems that essentially measure the noise in context of the thermal detectors. Thermal noise, which varies with temperature fluctuations, is the dominant noise source in thermal detectors. Note that the detector readout techniques and the FPA architectures (monolithic or hybrid) directly affect the noise performance of the system. When calculating overall S/N, all noise sources must be taken into consideration, the three prominent ones being the photon noise, dark noise, and read noise. Photon noise, also known as the shot noise, arises from the inherent statistical fluctuations in the arrival rate of the incident photons and can be calculated as $M_x\eta Pt$, in which P is the photon flux. Flicker noise is another type of electronic noise that is found in all active electronic devices and is caused by impurities in conductive channel, generation, and recombination noise in transistors. It is a low-frequency noise and is associated with a $1/f$ power spectral density. The S/N for a quantum detector can, thus, be estimated by Eq. 17, where noise is a quadratic sum of shot noise, readout noise, and the dark noise. Since the temperature fluctuation noise and the flicker noise are low compared to the photon noise and other noise sources, the equation can be summarized as

$$SNR = \frac{M_x\eta Pt}{\sqrt{M_x\eta(P + B)t + Dt + N_r^2}} \quad (17)$$

where N_r is the read noise, which is inherent to the process of converting the charge carrier into a voltage signal. The efficiency of this process is quantified by η and the integration time is denoted as t. The dark noise is D, the thermally generated photon count in the absence of any incident illumination, which is affected by the detector temperature and can be reduced further by cooling the substrate in many high-end systems. The noise floor is denoted by the background noise as B. Additionally, noise levels can be reduced through multiple measurements, often by averaging adjacent pixels to improve the S/N, where M_x represents the number of binned pixels. Under low-light conditions, when the read noise is greater than photon noise, the signal is considered to be read-noise limited, as shown in Fig. 12b. The exposure time can be increased to collect more photons and increase S/N, until a point is reached at which photon noise exceeds both read noise and dark noise. Above this exposure time, the image is said to be photon-noise limited. The two limitations specific to the performance of IR detectors are the temperature fluctuation noise and background fluctuation noise, which is determined by the photon shot noise.[233,234]

In any photon-noise limited system, a trade-off exists between (spatial, temporal, and spectral) resolution and S/N since the acquisition bins or times can be increased to perform signal averaging. Additionally, techniques such as compressed sensing can be used to acquire data at higher spatial frequencies resulting in images with finer spatial resolution but restricted S/N. A 100% line, which characterizes the spectral response of an instrument without a sample, is often used to estimate the noise in FT-IR spectrometers by calculating the ratio of two successive background spectra taken under identical conditions. In principle, the result is a flat line at 0% absorbance (100% transmission) and is a good indicator of the spectrum-to-spectrum consistency as well as the system spectral noise. Notably, the distribution of the averaged signal and the time period over which the 100% line is calculated also affects this analysis. As experimentally measured in Fig. 13a, the 100% line for the linear array and FPA-based FT-IR imaging spectrometers generally exhibit lower noise than the representative QCL-based widefield DFIR instrument. The advantages of an FT-IR instrument such as multiplexed measurements, thermal source stability and spectrally matched optical components and detector in terms of both throughput and capacity to the source, are well established. Taken altogether, they all serve to counter the unique advantages of a DFIR system, which hinge on the availability of a laser source with high spectral intensity as compared to a thermal source. Thus, we emphasize here that a complete design, choice of components and their careful matching leads to optimal performance. Comparison of instruments based on the strength of a single hardware component is not prudent. Similarly, a combined analysis of both the spectral and spatial
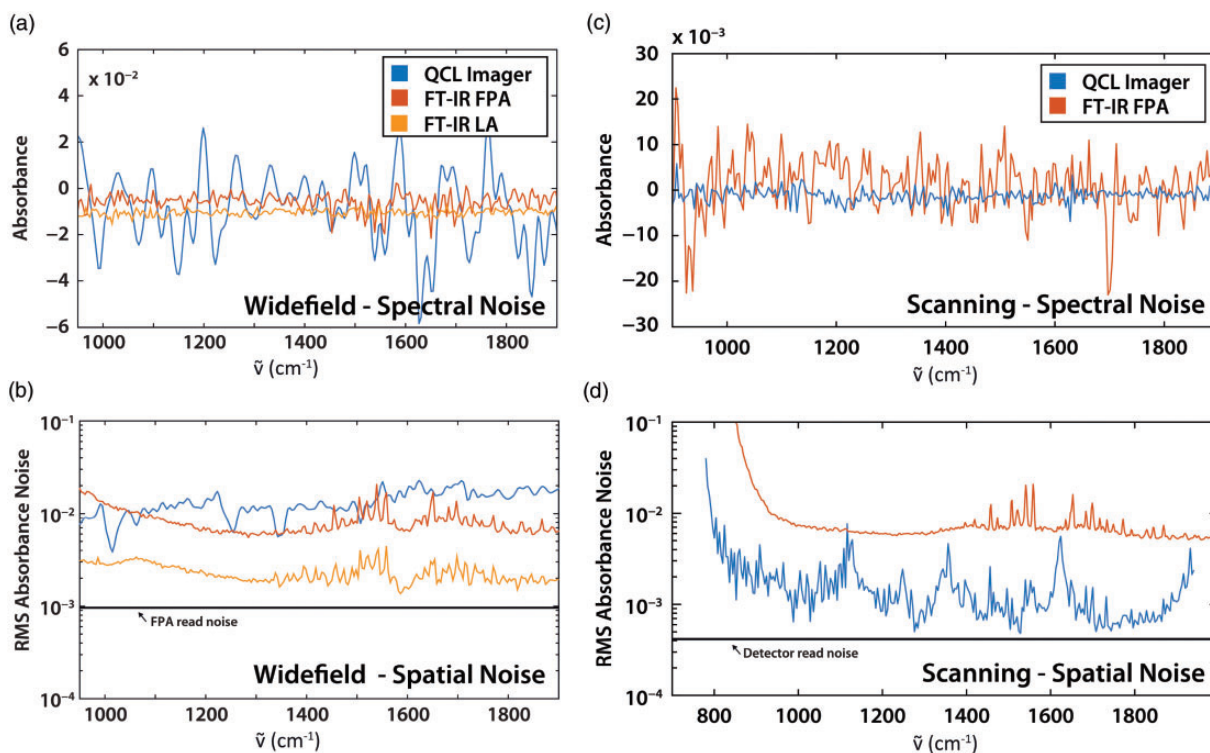
Figure 13. Comparison of the noise characteristics of IR imaging spectrometers. (a) Spatial RMS noise calculated using spatial variance of recorded data at each band in a hyperspectral image of a representative widefield DFIR and commercial FT-IR imaging systems. (b) 100% spectral lines from a single-pixel under typical experimental conditions and the corresponding FPA noise floor. Reproduced with permission from the Yeh et al.[132] Copyright 2014 American Chemical Society. (c) Spatial RMS noise calculated using spatial variance of recorded data at each band in a hyperspectral image of a representative DFIR point-scanning and commercial FT-IR imaging systems. (d) 100% spectral lines from a single-pixel under typical experimental conditions and the detector noise floor. Reproduced with permission from Yeh et al.[135] Copyright 2019 American Chemical Society.

performance should be undertaken to characterize a DFIR imaging system.

Noise in the 100% line can be safely assumed to be the analytical noise at any wavenumber in a DFIR spectrometer as each spectral point contributes to the noise at every spatial location. Thus, temporal variance at a wavenumber is the primary driver of noise, manifest in the spatial and spectral domains. Unlike FT-IR spectrometers where the FT explicitly relates spectral and temporal noise of the source, DFIR sources can present noise that varies across the spectrum. Given that most widely tunable QCL systems are composed of multiple chips, uniform performance across their bandwidths and consistency across the changeovers in both signal and noise is not guaranteed. Sensor nonuniformity of the staring array provides a spatial noise for widefield FT-IR imaging systems, which is also present in widefield DFIR systems but not in point detection systems. We did not observe an effect of shot noise, as shown by the root mean square (RMS) absorbance for each wavenumber in Fig. 13b, but it will become a crucial factor as more sensitive measurements are made. A scanning DFIR point-detection system has various sources of noise, mainly spectral noise and other minor contributions arising from

variations in the image, focusing, and spatial noise contributions arising from errors in stage motion. With matched optical design and careful system optimization, the total noise in a DFIR scanning system has been shown to be lower than that measured by a commercial FT-IR imaging spectrometer, as shown in Fig. 13c. This is an important comparison as FT instruments obviated scanning monochromators that used the same source, whereas the higher intensity of the QCL provides a competitive system if properly designed to take maximum advantage of the intrinsic characteristics of the laser source. Similarly, the RMS noise of each band for similar fields of view is shown in Fig. 13d. As in the previous case, the spectral noise for FT-IR instrument is constant and coupled to the temporal noise. However, noise contributions from water vapor lines fluctuations between 1300 to 2000 cm^{-1} and from the detector, below 1000 cm^{-1}, which is closer to the detector's spectral cut-off, tend to increase the spatial noise in both the cases. Just as standardized morphologies such as USAF resolution test chart, star, and line grating targets are used for spatial quality assessment, we urge the use of objective spectral performance using 100% lines, while specifying the optical configuration and experimental

conditions, to compare and quantify the performance of IR imaging systems.

Conclusion

In this review, we have summarized how resolution, aberrations, and S/N performance metrics can be used to validate current DFIR imaging system designs. When compared to the visual domain systems that are currently in use, DFIR systems are early in their development lifecycle and we expect to see more variants than the few available today. As technology progresses, we will need to incorporate additional metrics and procedures. For instance, a set of instruments may include laser scanning capabilities, which will necessitate measurements that can quantify image distortions over an FOV. Other potential techniques such as structured illumination and spatial modulation will similarly require specialized characterization methods. There are also application-specific considerations, such as for tissue classification tasks that users may wish to define spectral distance functions that further characterize the spectral separability potential of an instrument. Additionally, there are human operator and commercial vendor considerations which might affect performance. Finally, temporal variation should be considered as it is common for systems to evolve in time due to environmental changes, such as temperature and humidity. With a comprehensive description of the hardware and operational details, significant factors for comparison of imaging performance, and discussion of various experimental variables, these collated insights should prove useful in understanding imaging systems.

The last decade has seen the emergence and advancements in the performance of DFIR microscopy, which have been possible because of key factors, namely, the development and prevalence of high-speed, high-performance IR detectors[235] and high-powered, widely tunable QCL arrays. Additionally, with purpose-driven instrument design, including new optics, electronics, and control schemes, new DFIR imaging systems have demonstrated a considerable improvement in image quality while achieving a reduction in acquisition times. The technology has pushed IR spectroscopic imaging beyond previously foreseeable limits, while mathematical modeling, simulations, and analytical methods have improved our understanding of the acquired data. There are several factors that portend advances in IR imaging. Algorithmic inference coupled with rigorous mathematical models is now allowing a better understanding of the physics of image formation and effect of optical components. Co-design of hardware and software is enabling improvements in terms of faster image acquisition at higher quality. However, IR microscopy is still hindered by the selection and availability of components designed specifically for the mid- to far-IR spectral range, including optics, sources, and detectors. Advances in

manufacturing and prototyping across a range of industries will continue to make new capabilities more accessible. Due to this wide wavelength regime, use of the diversity of these technologies typically requires systematic component selection considerations and affords new opportunities for innovation by optimizing designs for particular performance needs. With a clear understanding of these considerations and their interplay, as summarized in this manuscript, the development and the miscellany of new IR spectroscopic instruments can lead to newer applications and greater understanding of structure–property relationships that are central to applied spectroscopy.

ORCID iD

Rohit Bhargava   https://orcid.org/0000-0001-7360-994X

References

1. R. Barer, A. Cole, H. Thompson. "Infrared Spectroscopy with the Reflecting Microscope in Physics, Chemistry, and Biology". Nature. 1949. 163(4136): 198–201.
2. V.J. Coates, A. Offner, E. Siegler. "Design and Performance of an Infrared Microscope Attachment". J. Opt. Soc. Am. 1953. 43(11): 984–989.
3. J.A. Reffner, P.A. Martoglio, G.P. Williams. "Fourier Transform Infrared Microscopical Analysis with Synchrotron Radiation: The Microscope Optics and System Performance". Rev. Sci. Instrum. 1995. 66(2): 1298–1302.
4. R. Bhargava. "Infrared Spectroscopic Imaging: The Next Generation". Appl. Spectrosc. 2012. 66(10): 1091–1120.
5. A.K. Kodali, M. Schulmerich, J. Ip, G. Yen, B.T. Cunningham, et al. "Narrowband Mid-Infrared Reflectance Filters Using Guided Mode Resonance". Anal. Chem. 2010. 82(13): 5697–5706.
6. J.-N. Liu, M.V. Schulmerich, R. Bhargava, B.T. Cunningham. "Optimally Designed Narrowband Guided-Mode Resonance Reflectance Filters for Mid-Infrared Spectroscopy". Opt. Express. 2011. 19(24): 24182–24197.
7. J.-N. Liu, M.V. Schulmerich, R. Bhargava, B.T. Cunningham. "Sculpting Narrowband Fano Resonances Inherent in the Large-Area Mid-Infrared Photonic Crystal Microresonators for Spectroscopic Imaging". Opt. Express. 2014. 22(15): 18142–18158.
8. J. Faist, F. Capasso, D.L. Sivco, C. Sirtori, A.L. Hutchinson, et al. "Quantum Cascade Laser". Science. 1994. 264(5158): 553–556.

9. B.G. Lee, M.A. Belkin, R. Audet, J. MacArthur, L. Diehl, et al. "Widely Tunable Single-Mode Quantum Cascade Laser Source for Mid-Infrared Spectroscopy". Appl. Phys. Lett. 2007. 91(23): 231101.

10. Y. Yao, A.J. Hoffman, C.F. Gmachl. "Mid-Infrared Quantum Cascade Lasers". Nat. Photonics. 2012. 6(7): 432–439.

11. N. Yu, F. Capasso. "Flat Optics with Designer Metasurfaces". Nat. Mater. 2014. 13(2): 139–150.

12. M. Meem, S. Banerji, A. Majumder, F.G. Vasquez, B. Sensale-Rodriguez, et al. "Broadband Lightweight Flat Lenses for Long-Wave Infrared Imaging". Proc. Natl. Acad. Sci. U.S.A. 2019. 116(43): 21375–21378.

13. D.M. Price, M. Reading, A. Hammiche, H.M. Pollock. "Micro-Thermal Analysis: Scanning Thermal Microscopy and Localised Thermal Analysis". Int. J. Pharm. 1999. 192(1): 85–96.

14. A. Hammiche, L. Bozec, M. German, J. Chalmers, N. Everall, et al. "Mid-Infrared Microspectroscopy of Difficult Samples Using Near-Field Photothermal Microspectroscopy". Spectroscopy. 2004. 19(2): 20–42.

15. A. Hammiche, D. Price, E. Dupas, G. Mills, A. Kulik, et al. "Two New Microscopical Variants of Thermomechanical Modulation: Scanning Thermal Expansion Microscopy and Dynamic Localized Thermomechanical Analysis". J. Microsc. 2000. 199(3): 180–190.

16. G.A. Hill, J.H. Rice, S.R. Meech, D.Q. Craig, P. Kuo, et al. "Submicrometer Infrared Surface Imaging Using a Scanning-Probe Microscope and an Optical Parametric Oscillator Laser". Opt. Lett. 2009. 34(4): 431–433.

17. A. Dazzi, C.B. Prater, Q. Hu, D.B. Chase, J.F. Rabolt, et al. "AFM-IR: Combining Atomic Force Microscopy and Infrared Spectroscopy for Nanoscale Chemical Characterization". Appl. Spectrosc. 2012. 66(12): 1365–1384.

18. J.H. Rice. "Nanoscale Optical Imaging by Atomic Force Infrared Microscopy". Nanoscale. 2010. 2(5): 660–667.

19. F. Yarrow, E. Kennedy, F. Salaun, J.H. Rice. "Sub-Wavelength Infrared Imaging of Lipids". Biomed. Opt. Express. 2011. 2(1): 37–43.

20. A. Dazzi, C.B. Prater. "AFM-IR: Technology and Applications in Nanoscale Infrared Spectroscopy and Chemical Imaging". Chem. Rev. 2017. 117(7): 5146–5173.

21. F. Huth, M. Schnell, J. Wittborn, N. Ocelic, R. Hillenbrand. "Infrared Spectroscopic Nanoimaging with a Thermal Source". Nat. Mater. 2011. 10(5): 352–356.

22. J. Houel, E. Homeyer, S. Sauvage, P. Boucaud, A. Dazzi, et al. "Mid-Infrared Absorption Measured at a $\lambda/400$ Resolution with an Atomic Force Microscope". Opt. Express. 2009. 17(13): 10887–10894.

23. D. Kurouski, A. Dazzi, R. Zenobi, A. Centrone. "Infrared and Raman Chemical Imaging and Spectroscopy at the Nanoscale". Chem. Soc. Rev. 2020. 49(11): 3315–3347.

24. O. Khatib, H.A. Bechtel, M.C. Martin, M.B. Raschke, G.L. Carr. "Far-Infrared Synchrotron Near-Field Nanoimaging and Nanospectroscopy". ACS Photonics. 2018. 5(7): 2773–2779.

25. I. Amenabar, S. Poly, M. Goikoetxea, W. Nuansing, P. Lasch, et al. "Hyperspectral Infrared Nanoimaging of Organic Samples Based on Fourier Transform Infrared Nanospectroscopy". Nat. Commun. 2017. 8(1): 1–10.

26. A. Mertiri, T. Jeys, V. Liberman, M. Hong, J. Mertz, et al. "Mid-Infrared Photothermal Heterodyne Spectroscopy in a Liquid Crystal Using a Quantum Cascade Laser". Appl. Phys. Lett. 2012. 101(4): 044101.

27. Z. Li, K. Aleshire, M. Kuno, G.V. Hartland. "Super-Resolution Far-Field Infrared Imaging by Photothermal Heterodyne Imaging". J. Phys. Chem. B. 2017. 121(37): 8838–8846.

28. A. Mertiri, H. Altug, M.K. Hong, P. Mehta, J. Mertz, et al. "Nonlinear Mid-Infrared Photothermal Spectroscopy Using Zharov Splitting and Quantum Cascade Lasers". ACS Photonics. 2014. 1(8): 696–702.

29. M.Y. Sander. "Mid-Infrared Photothermal Imaging". In: Laser Science. San Jose, CA; October 18–22, 2015. Paper LM1I.2.

30. R. Chatterjee, I.M. Pavlovetc, K. Aleshire, G.V. Hartland, M. Kuno. "Sub-Diffraction Infrared Imaging of Mixed Cation Perovskites: Probing Local Cation Heterogeneities". ACS Energy Lett. 2018. 3(2): 469–475.

31. Y. Bai, D. Zhang, C. Li, C. Liu, J.-X. Cheng. "Bond-Selective Imaging of Cells by Mid-Infrared Photothermal Microscopy in High Wavenumber Region". J. Phys. Chem. B. 2017. 121(44): 10249–10255.

32. Y. Bai, D. Zhang, L. Lan, Y. Huang, K. Maize, et al. "Ultrafast Chemical Imaging by Widefield Photothermal Sensing of Infrared Absorption". Sci. Adv. 2019. 5(7): eaav7127.

33. M. Schnell, S. Mittal, K. Falahkheirkhah, A. Mittal, K. Yeh, et al. "All-Digital Histopathology by Infrared-Optical Hybrid Microscopy". Proc. Natl. Acad. Sci. U.S.A. 2020. 117(7): 3388–3396.

34. M. Tamamitsu, K. Toda, H. Shimada, T. Honda, M. Takarada, et al. "Label-Free Biochemical Quantitative Phase Imaging with Mid-Infrared Photothermal Effect". Optica. 2020. 7(4): 359–366.

35. D. Knez, A.M. Hanninen, R.C. Prince, E.O. Potma, D.A. Fishman. "Infrared Chemical Imaging Through Nondegenerate Two-Photon Absorption in Silicon-Based Cameras". Light: Sci. Appl. 2020. 9. 1: 1–10.

36. M.A. Pleitez, A.A. Khan, A. Solda, A. Chmyrov, J. Reber, et al. "Label-Free Metabolic Imaging by Mid-Infrared Optoacoustic Microscopy in Living Cells". Nat. Biotechnol. 2020. 38(3): 293–296.

37. J. Shi, T.T. Wong, Y. He, L. Li, R. Zhang, et al. "High-Resolution, High-Contrast Mid-Infrared Imaging of Fresh Biological Samples with Ultraviolet-Localized Photoacoustic Microscopy". Nat. Photonics. 2019. 13(9): 609–615.

38. S. Kenkel, S. Mittal, R. Bhargava. "Closed-Loop Atomic Force Microscopy-Infrared Spectroscopic Imaging for Nanoscale Molecular Characterization". Nat. Commun. 2020. 11(1): 1–10.

39. A. Dazzi, F. Glotin, R. Carminati. "Theory of Infrared Nanospectroscopy by Photothermal Induced Resonance". J. Appl. Phys. 2010. 107. 12: 124519.

40. H.-J. Butt, B. Cappella, M. Kappl. "Force Measurements with the Atomic Force Microscope: Technique, Interpretation and Applications". Surf. Sci. Rep. 2005. 59(1–6): 1–152.

41. R. Fraser. "Infrared Microspectrometry with a 0. 8NA Reflecting Microscope". Discuss. Faraday Soc. 1950. 9: 378–383.

42. E.R. Blout, G.R. Bird, D.S. Grey. "Infrared Microspectroscopy". J. Opt. Soc. Am. 1950. 40(5): 304–313.

43. R.M. Badger, R. Newman. "A Microilluminator for the Study of the Infrared Spectra of Small Samples at Low Temperatures". Rev. Sci. Instrum. 1951. 22(12): 935–936.

44. R. Gore. "Infrared Spectrometry of Small Samples with the Reflecting Microscope". Science. 1949. 110(2870): 710–711.

45. D.L. Elmore, M.-W. Tsao, S. Frisk, D.B. Chase, J.F. Rabolt. "Design and Performance of a Planar Array Infrared Spectrograph that Operates in the 3400 to 2000 cm^{-1} Region". Appl. Spectrosc. 2002. 56(2): 145–149.

46. C. Pellerin, C.M. Snively, D.B. Chase, J.F. Rabolt. "Performance and Application of a New Planar Array Infrared Spectrograph Operating in the Mid-Infrared (2000–975 cm^{-1}) Fingerprint Region". Appl. Spectrosc. 2004. 58(6): 639–646.

47. M.E. Gehm, S.T. McCain, N.P. Pitsianis, D.J. Brady, P. Potuluri, et al. "Static Two-Dimensional Aperture Coding for Multimodal, Multiplex Spectroscopy". Appl. Opt. 2006. 45(13): 2965–2974.

48. P.R. Griffiths, J.A. De Haseth. Fourier Transform Infrared Spectrometry. Hoboken, NJ: John Wiley and Sons, 2007. P. 171.

49. J. Kwiatkoski, J. Reffner. "FT-IR Microspectrometry Advances". Nature. 1987. 328(6133): 837–838.

50. R.G. Messerschmidt, M.A. Harthcock. Infrared Microspectroscopy. Theory and Applications. New York: Marcel Dekker, 1988.

51. H.J. Humecki. Practical Guide to Infrared Microspectroscopy. Boca Raton: CRC Press, 1995.

52. J. Reffner. "Instrumental Factors in Infrared Microspectroscopy". Cell. Mol. Biol. 1998. 44(1): 1–7.

53. A. Dong, R.G. Messerschmidt, J.A. Reffner, W.S. Caughey. "Infrared Spectroscopy of a Single Cell: The Human Erythrocyte". Biochem. Biophys. Res. Commun. 1988. 156(2): 752–756.

54. D.L. Wetzel, S.M. LeVine. "Imaging Molecular Chemistry with Infrared Microscopy". Science. 1999. 285(5431): 1224–1225.

55. G.L. Carr, J. Reffner, G. Williams. "Performance of an Infrared Microspectrometer at the NSLS". Rev. Sci. Instrum. 1995. 66(2): 1490–1492.

56. G.L. Carr, G.P. Williams. "Infrared Microspectroscopy with Synchrotron Radiation". In: G.P. Williams, P. Dumas, editors. Accelerator-Based Infrared Sources and Applications. San Diego, California; 1997. Vol. 3153, Pp. 51–58.

57. P. Dumas, N. Jamin, J. Teillaud, L. Miller, B. Beccard. "Imaging Capabilities of Synchrotron Infrared Microspectroscopy". Faraday Discuss. 2004. 126: 289–302.

58. L.M. Miller, P. Dumas. "Chemical Imaging of Biological Tissue with Synchrotron Infrared Light". Biochim. Biophys. Acta, Biomembr. 2006. 1758(7): 846–857.

59. N.S. Marinkovic, M.R. Chance. "Synchrotron Infrared Microspectroscopy". In: Reviews in Cell Biology and Molecular Medicine. Weinheim, Germany: Wiley-VCH, 2006. Pp. 671–700.

60. P. Dumas, G.D. Sockalingum, J. Sule-Suso. "Adding Synchrotron Radiation to Infrared Microspectroscopy: What's New in Biomedical Applications?" Trends Biotechnol. 2007. 25(1): 40–44.

61. D. Moss. Biomedical Applications of Synchrotron Infrared Microspectroscopy: A Practical Approach. Cambridge, UK: Royal Society of Chemistry, 2011.

62. H.-Y.N. Holman, H.A. Bechtel, Z. Hao, M.C. Martin. "Synchrotron IR Spectromicroscopy: Chemistry of Living Cells". Anal. Chem. 2010. 82(21): 8757–8765.

63. R. Bosch. "Focusing Infrared Edge and Synchrotron Radiation with a Large Numerical Aperture". Nucl. Instrum. Methods Phys. Res., Sect. A. 2002. 492(1–2): 284–298.

64. N. Jamin, P. Dumas, J. Moncuit, W.-H. Fridman, J.-L. Teillaud, et al. "Highly Resolved Chemical Imaging of Living Cells by Using Synchrotron Infrared Microspectrometry". Proc. Natl. Acad. Sci. U.S.A. 1998. 95(9): 4837–4840.

65. P. Dumas, L. Miller. "The Use of Synchrotron Infrared Microspectroscopy in Biological and Biomedical Investigations". Vib. Spectrosc. 2003. 32(1): 3–21.

66. G. Carr. "Resolution Limits for Infrared Microspectroscopy Explored with Synchrotron Radiation". Rev. Sci. Instrum. 2001. 72(3): 1613–1619.

67. L. Vaccari, G. Birarda, G. Grenci, S. Pacor, L. Businaro. "Synchrotron Radiation Infrared Microspectroscopy of Single Living Cells in Microfluidic Devices: Advantages, Disadvantages, and Future Perspectives". J. Phys.: Conf. Ser. 2012. 359(1): 012007.

68. K. Loutherback, G. Birarda, L. Chen, H.-Y.N. Holman. "Microfluidic Approaches to Synchrotron Radiation-Based Fourier Transform Infrared (SR-FT-IR) Spectral Microscopy of Living Biosystems". Protein Pept. Lett. 2016. 23(3): 273–282.

69. E.N. Lewis, P.J. Treado, R.C. Reeder, G.M. Story, A.E. Dowrey, et al. "Fourier Transform Spectroscopic Imaging Using an Infrared Focal-Plane Array Detector". Anal. Chem. 1995. 67(19): 3377–3381.

70. L.H. Kidder, V.F. Kalasinsky, J.L. Luke, I.W. Levin, E.N. Lewis. "Visualization of Silicone Gel in Human Breast Tissue Using New Infrared Imaging Spectroscopy". Nat. Med. 1997. 3(2): 235–237.

71. C. Snively, S. Katzenberger, G. Oskarsdottir, J. Lauterbach. "Fourier Transform Infrared Imaging Using a Rapid-Scan Spectrometer". Opt. Lett. 1999. 24(24): 1841–1843.

72. S.W. Huffman, R. Bhargava, I.W. Levin. "Generalized Implementation of Rapid-Scan Fourier Transform Infrared Spectroscopic Imaging". Appl. Spectrosc. 2002. 56(8): 965–969.

73. R. Bhargava, I.W. Levin. "Time-Resolved Fourier Transform Infrared Spectroscopic Imaging". Appl. Spectrosc. 2003. 57(4): 357–366.

74. M.J. Nasse, M.J. Walsh, E.C. Mattson, R. Reininger, A. Kajdacsy-Balla, et al. "High-Resolution Fourier-Transform Infrared Chemical Imaging with Multiple Synchrotron Beams". Nat. Methods. 2011. 8(5): 413–416.

75. C.M. Snively, G. Oskarsdottir, J. Lauterbach. "Chemically Sensitive Parallel Analysis of Combinatorial Catalyst Libraries". Catal. Today. 2001. 67(4): 357–368.

76. R. Bhargava, S.-Q. Wang, J.L. Koenig. "FT-IR Microspectroscopy of Polymeric Systems". In: Advances in Polymer Science. Berlin; Heidelberg: Springer, 2003. Vol. 163, Pp. 137–191.

77. I.W. Levin, R. Bhargava. "Fourier Transform Infrared Vibrational Spectroscopic Imaging: Integrating Microscopy and Molecular Recognition". Annu. Rev. Phys. Chem. 2005. 56: 429–474.

78. C. Petibois, G. Deleris. "Chemical Mapping of Tumor Progression by FT-IR Imaging: Towards Molecular Histopathology". Trends Biotechnol. 2006. 24(10): 455–462.

79. S.G. Kazarian, K.L.A. Chan. "Applications of ATR FT-IR Spectroscopic Imaging to Biomedical Samples". Biochim. Biophys. Acta, Biomembr. 2006. 1758(7): 858–867.

80. S.G. Kazarian. "Perspectives on Infrared Spectroscopic Imaging from Cancer Diagnostics to Process Analysis". Spectrochim. Acta, Part A. 2021. 251: 119413.

81. P. Heraud, S. Caine, G. Sanson, R. Gleadow, B.R. Wood, et al. "Focal Plane Array Infrared Imaging: A New Way to Analyse Leaf Tissue". New Phytol. 2007. 173(1): 216–225.

82. G. Steiner, E. Koch. "Trends in Fourier Transform Infrared Spectroscopic Imaging". Anal. Bioanal. Chem. 2009. 394(3): 671–678.

83. G. Bellisola, M.D. Peruta, M. Vezzalini, E. Moratti, L. Vaccari, et al. "Tracking Infrared Signatures of Drugs in Cancer Cells by Fourier Transform Microspectroscopy". Analyst. 2010. 135(12): 3077–3086.

84. R. Kong, R.K. Reddy, R. Bhargava. "Characterization of Tumor Progression in Engineered Tissue Using Infrared Spectroscopic Imaging". Analyst. 2010. 135(7): 1569–1578.

85. G. Bellisola, C. Sorio. "Infrared Spectroscopy and Microscopy in Cancer Research and Diagnosis". Am. J. Cancer Res. 2012. 2(1): 1–21.

86. S. Kumar, C. Desmedt, D. Larsimont, C. Sotiriou, E. Goormaghtigh. "Change in the Microenvironment of Breast Cancer Studied by FT-IR Imaging". Analyst. 2013. 138(14): 4058–4065.

87. K.M. Dorling, M.J. Baker. "Rapid FT-IR Chemical Imaging: Highlighting FPA Detectors". Trends Biotechnol. 2013. 31(8): 437–438.

88. K. Malek, B.R. Wood, K.R. Bambery. "FT-IR Imaging of Tissues: Techniques and Methods of Analysis". In: M. Baranska, editor. Optical Spectroscopy and Computational Methods in Biology and Medicine. Challenges and Advances in Computational Chemistry and Physics. Dordrecht: Springer, 2014. Chap. 14, Pp. 419–473.

89. S. Pahlow, K. Weber, J. Popp, R.W. Bayden, K. Kochan, et al. "Application of Vibrational Spectroscopy and Imaging to Point-of-Care Medicine: A Review". Appl. Spectrosc. 2018. 72(101): 52–84.

90. R. Bhargava, B.G. Wall, J.L. Koenig. "Comparison of the FT-IR Mapping and Imaging Techniques Applied to Polymeric Systems". Appl. Spectrosc. 2000. 54(4): 470–479.

91. L.M. Miller, R.J. Smith. "Synchrotrons Versus Globars, Point-Detectors Versus Focal Plane Arrays: Selecting the Best Source and Detector for Specific Infrared Microspectroscopy and Imaging Applications". Vib. Spectrosc. 2005. 38(1–2): 237–240.

92. R. Bhargava, T. Ribar, J.L. Koenig. "Towards Faster FT-IR Imaging by Reducing Noise". Appl. Spectrosc. 1999. 53(11): 1313–1322.

93. R. Bhargava, S.-Q. Wang, J.L. Koenig. "Route to Higher Fidelity FT-IR Imaging". Appl. Spectrosc. 2000. 54(4): 486–495.

94. R. Bhargava, I.W. Levin. Spectrochemical Analysis Using Infrared Multichannel Detectors. UK: John Wiley and Sons, 2008.

95. T. Ribar, J.L. Koenig, R. Bhargava. "FT-IR Imaging of Polymer Dissolution. 2. Solvent/Nonsolvent Mixtures". Macromolecules. 2001. 34(23): 8340–8346.

96. S.G. Kazarian, K.L.A. Chan. "'Chemical Photography' of Drug Release". Macromolecules. 2003. 36(26): 9866–9872.

97. R. Bhargava, I.W. Levin. "Noninvasive Imaging of Molecular Dynamics in Heterogeneous Materials". Macromolecules. 2003. 36(1): 92–96.

98. C.M. Snively, G. Oskarsdottir, J. Lauterbach. "Parallel Analysis of the Reaction Products from Combinatorial Catalyst Libraries". Angew. Chem., Int. Ed. 2001. 40(16): 3028–3030.

99. D. Fernandez, R. Bhargava, S. Hewitt, I. Levin. "Infrared Spectroscopic Imaging for Observer-Invariant Histopathology". Nat. Biotechnol. 2005. 23: 469–474.

100. M.C. Martin, C. Dabat-Blondeau, M. Unger, J. Sedlmair, D.Y. Parkinson, et al. "3D Spectral Imaging with Synchrotron Fourier Transform Infrared Spectro-Microtomography". Nat. Methods. 2013. 10(9): 861–864.

101. R. Reddy, D. Mayerich, M. Walsh, M. Schulmerich, P.S. Carney, et al. "Optimizing the Design of FT-IR Spectroscopic Imaging Instruments to Obtain Increased Spatial Resolution of Chemical Species". In: 2012 9th IEEE International Symposium on Biomedical Imaging (ISBI). IEEE, Barcelona, Spain; May 2–5, 2012. Pp. 354–357.

102. K.L.A. Chan, S.G. Kazarian. "Aberration-Free FT-IR Spectroscopic Imaging of Live Cells in Microfluidic Devices". Analyst. 2013. 138(14): 4040–4047.

103. S.G. Kazarian, K.L.A. Chan. "ATR FT-IR Spectroscopic Imaging: Recent Advances and Applications to Biological Systems". Analyst. 2013. 138(7): 1940–1951.

104. S.E. Glassford, B. Byrne, S.G. Kazarian. "Recent Applications of ATR FT-IR Spectroscopy and Imaging to Proteins". Biochim. Biophys. Acta, Proteins Proteomics. 2013. 1834(12): 2849–2858.

105. K.L.A. Chan, S.G. Kazarian. "New Opportunities in Micro- and Macro-Attenuated Total Reflection Infrared Spectroscopic Imaging: Spatial Resolution and Sampling Versatility". Appl. Spectrosc. 2003. 57(4): 381–389.

106. S.G. Kazarian, K.L.A. Chan. "Micro- and Macro-Attenuated Total Reflection Fourier Transform Infrared Spectroscopic Imaging". Appl. Spectrosc. 2010. 64(5): 135A–152A.

107. K.L.A. Chan, S.G. Kazarian. "Attenuated Total Reflection Fourier-Transform Infrared (ATR FT-IR) Imaging of Tissues and Live Cells". Chem. Soc. Rev. 2016. 45(7): 1850–1864.

108. K.L.A. Chan, S. Gulati, J.B. Edel, A.J. de Mello, S.G. Kazarian. "Chemical Imaging of Microfluidic Flows Using ATR FT-IR Spectroscopy". Lab Chip. 2009. 9(20): 2909–2913.

109. R.K. Reddy, M.J. Walsh, M.V. Schulmerich, P.S. Carney, R. Bhargava. "High-Definition Infrared Spectroscopic Imaging". Appl. Spectrosc. 2013. 67(1): 93–105.

110. C.J. Hirschmugl, K.M. Gough. "Fourier Transform Infrared Spectrochemical Imaging: Review of Design and Applications with a Focal Plane Array and Multiple Beam Synchrotron Radiation Source". Appl. Spectrosc. 2012. 66(5): 475–491.

111. P. Gelfand, R.J. Smith, E. Stavitski, D.R. Borchelt, L.M. Miller. "Characterization of Protein Structural Changes in Living Cells Using Time-Lapsed FT-IR Imaging". Anal. Chem. 2015. 87(12): 6025–6031.

112. L.S. Leslie, A. Kadjacsy-Balla, R. Bhargava. "High-Definition Fourier Transform Infrared Spectroscopic imaging of Breast Tissue". In: Medical Imaging 2015: Digital Pathology. 2015. Vol. 9420, P. 94200I.

113. M. Hermes, R.B. Morrish, L. Huot, L. Meng, S. Junaid, et al. "Mid-IR Hyperspectral Imaging for Label-Free Histopathology and Cytology". J. Opt. 2018. 20(2): 023002.

114. M. Kastyak-Ibrahim, M. Nasse, M. Rak, C. Hirschmugl, S. Del Bigio, et al. "Biochemical Label-Free Tissue Imaging with Subcellular-Resolution Synchrotron FT-IR with Focal Plane Array Detector". NeuroImage. 2012. 60(1): 376–383.

115. C.R. Findlay, R. Wiens, M. Rak, J. Sedlmair, C. Hirschmugl, et al. "Rapid Biodiagnostic Ex Vivo Imaging at 1 μm Pixel Resolution with Thermal Source FT-IR FPA". Analyst. 2015. 140(7): 2493–2503.

116. M.J. Walsh, R.K. Reddy, R. Bhargava. "Label-Free Biomedical Imaging with Mid-IR Spectroscopy". IEEE J. Sel. Top. Quantum Electron. 2012. 18(4): 1502–1513.

117. J. Nallala, G.R. Lloyd, N. Shepherd, N. Stone. "High-Resolution FT-IR Imaging of Colon Tissues for Elucidation of Individual Cellular and Histopathological Features". Analyst. 2016. 141(2): 630–639.

118. J. Nallala, G.R. Lloyd, M. Hermes, N. Shepherd, N. Stone. "Enhanced Spectral Histology in the Colon Using High-Magnification Benchtop FT-IR Imaging". Vib. Spectrosc. 2017. 91: 83–91.

119. K. Augustyniak, K. Chrabaszcz, A. Jasztal, M. Smeda, G. Quintas, et al. "High and Ultra-High Definition of Infrared Spectral Histopathology Gives an Insight into Chemical Environment of Lung Metastases in Breast Cancer". J. Biophotonics. 2019. 12(4): e201800345.

120. K. Chrabaszcz, K. Kochan, A. Fedorowicz, A. Jasztal, E. Buczek, et al. "FT-IR- and Raman-Based Biochemical Profiling of the Early Stage of Pulmonary Metastasis of Breast Cancer in Mice". Analyst. 2018. 143(9): 2042–2050.

121. S. Berisha, M. Lotfollahi, J. Jahanipour, I. Gurcan, M.J. Walsh, et al. "Deep Learning for FT-IR Histology: Leveraging Spatial and Spectral Features with Convolutional Neural Networks". Analyst. 2019. 144(5): 1642–1653.

122. M. Lotfollahi, S. Berisha, D. Daeinejad, D. Mayerich. "Digital Staining of High-Definition Fourier Transform Infrared (FT-IR) Images Using Deep Learning". Appl. Spectrosc. 2019. 73(5): 556–564.

123. H. Sreedhar, V.K. Varma, P.L. Nguyen, B. Davidson, S. Akkina, et al. "High-Definition Fourier Transform Infrared (FT-IR) Spectroscopic Imaging of Human Tissue Sections Towards Improving Pathology". J. Visualized Exp. 2015. 95: e52332.

124. B.J. Davis, P.S. Carney, R. Bhargava. "Theory of Mid-Infrared Absorption Microspectroscopy: I. Homogeneous Samples". Anal. Chem. 2010. 82(9): 3474–3486.

125. B.J. Davis, P.S. Carney, R. Bhargava. "Theory of Mid-Infrared Absorption Microspectroscopy: II. Heterogeneous Samples". Anal. Chem. 2010. 82(9): 3487–3499.

126. B.J. Davis, P.S. Carney, R. Bhargava. "Theory of Infrared Microspectroscopy for Intact Fibers". Anal. Chem. 2011. 83(2): 525–532.

127. T. Van Dijk, D. Mayerich, P.S. Carney, R. Bhargava. "Recovery of Absorption Spectra from Fourier Transform Infrared (FT-IR) Microspectroscopic measurements of Intact Spheres". Appl. Spectrosc. 2013. 67(5): 546–552.

128. D. Mayerich, T. Van Dijk, M.J. Walsh, M.V. Schulmerich, P.S. Carney, et al. "On the Importance of Image Formation Optics in the Design of Infrared Spectroscopic Imaging Systems". Analyst. 2014. 139(16): 4031–4036.

129. T.G. Mayerhofer, S. Pahlow, U. Hubner, J. Popp. "Removing Interference-Based Effects from the Infrared Transflectance Spectra of Thin Films on Metallic Substrates: A Fast and Wave Optics Conform Solution". Analyst. 2018. 143(13): 3164–3175.

130. T.G. Mayerhofer, S. Pahlow, U. Hubner, J. Popp. "Removing Interference-Based Effects from Infrared Spectra–Interference Fringes Re-Revisited". Analyst. 2020. 145(9): 3385–3394.

131. J. Rowlette, M. Weide, B. Bird, D. Arnone, M. Barre, et al. "High-Confidence, High-Throughput Screening with High-Def IR Microspectroscopy". BioOptics World. 2014. 7(2): 34–37.

132. K. Yeh, S. Kenkel, J.-N. Liu, R. Bhargava. "Fast Infrared Chemical Imaging with a Quantum Cascade Laser". Anal. Chem. 2014. 87(1): 485–493.

133. M.R. Kole, R.K. Reddy, M.V. Schulmerich, M.K. Gelber, R. Bhargava. "Discrete Frequency Infrared Microspectroscopy and Imaging with a Tunable Quantum Cascade Laser". Anal. Chem. 2012. 84(23): 10 366–10 372.

134. A. Schonhals, N. Kroger-Lui, A. Pucci, W. Petrich. "On the Role of Interference in Laser-Based Mid-Infrared Widefield Microspectroscopy". J. Biophotonics. 2018. 11(7): e201800015.

135. K. Yeh, D. Lee, R. Bhargava. "Multicolor Discrete Frequency Infrared Spectroscopic Imaging". Anal. Chem. 2019. 91(3): 2177–2185.

136. P. Bassan, M.J. Weida, J. Rowlette, P. Gardner. "Large Scale Infrared Imaging of Tissue Micro Arrays (TMAs) Using a Tunable Quantum

Cascade Laser (QCL) Based Microscope". Analyst. 2014. 139(16): 3856–3859.

137. N. Kroger, A. Egl, M. Engel, N. Gretz, K. Haase, et al. "Quantum Cascade Laser-Based Hyperspectral Imaging of Biological Tissue". J. Biomed. Opt. 2014. 19(11): 111607.

138. C. Kuepper, A. Kallenbach-Thieltges, H. Juette, A. Tannapfel, F. Großerueschkamp, et al. "Quantum Cascade Laser-Based Infrared Microscopy for Label-Free and Automated Cancer Classification in Tissue Sections". Sci. Rep. 2018. 8(1): 7717.

139. S. Ran, S. Berisha, R. Mankar, W.-C. Shih, D. Mayerich. "Mitigating Fringing in Discrete Frequency Infrared Imaging Using Time-Delayed Integration". Biomed. Opt. Express. 2018. 9(2): 832–843.

140. S. Tiwari, J. Raman, V. Reddy, A. Ghetler, R.P. Tella, et al. "Towards Translation of Discrete Frequency Infrared Spectroscopic Imaging for Digital Histopathology of Clinical Biopsy Samples". Anal. Chem. 2016. 88(20): 10183–10190.

141. S. Mittal, K. Yeh, L.S. Leslie, S. Kenkel, A. Kajdacsy-Balla, et al. "Simultaneous Cancer and Tumor Microenvironment Subtyping Using Confocal Infrared Microscopy for All-Digital Molecular Histopathology". Proc. Natl. Acad. Sci. U.S.A. 2018. 115(25): E5651–E5660.

142. M.C. Martin, N.M. Tsvetkova, J.H. Crowe, W.R. McKinney. "Negligible Sample Heating from Synchrotron Infrared Beam". Appl. Spectrosc. 2001. 55(2): 111–113.

143. H.Y. Holman, M.C. Martin, W.R. McKinney. "Synchrotron-Based FT-IR Spectromicroscopy: Cytotoxicity and Heating Considerations". J. Biol. Phys. 2003. 29(2): 275–286.

144. B. Guo, Y. Wang, C. Peng, G. Luo, H.Q. Le. "Multi-Wavelength Mid-Infrared Micro-Spectral Imaging Using Semiconductor Lasers". Appl. Spectrosc. 2003. 57(7): 811–822.

145. K. Yeh, R. Bhargava. "Discrete Frequency Infrared Imaging Using Quantum Cascade Lasers for Biological Tissue Analysis". In: Biomedical Vibrational Spectroscopy 2016: Advances in Research and Industry. USA: International Society for Optics and Photonics, 2016. Vol. 9704, P. 970406.

146. M. Endo, D.P. Robey, D. Minali, C. Moon. "LDIR Chemical Imaging System". Agilent Technologies, Inc., 2019. https://www.agilent.com/en/product/molecular-spectroscopy/ldir-chemical-imaging-spectroscopy/ldir-chemical-imaging-system/ldir-chemical-imaging-system [accessed May 19 2021].

147. P. Dumas, G.L. Carr, G.P. Williams. "Enhancing the Lateral Resolution in Infrared Microspectrometry by Using Synchrotron Radiation: Applications and Perspectives". Analusis. 2000. 28(1): 68–68.

148. C. Petibois, M. Piccinini, M. CestelliGuidi, G. Deleris, A. Marcelli. "Infrared Synchrotron Sources: A Boon for Biology". Nat. Photonics. 2009. 3: 177.

149. M.C. Martin, U. Schade, P. Lerch, P. Dumas. "Recent Applications and Current Trends in Analytical Chemistry Using Synchrotron-Based Fourier-Transform Infrared Microspectroscopy". TrAC, Trends Anal. Chem. 2010. 29(6): 453–463.

150. I. Coddington, W.C. Swann, N.R. Newbury. "Coherent Multiheterodyne Spectroscopy Using Stabilized Optical Frequency Combs". Phys. Rev. Lett. 2008. 100(1): 013902.

151. F. Keilmann, C. Gohle, R. Holzwarth. "Time-Domain Mid-Infrared Frequency-Comb Spectrometer". Opt. Lett. 2004. 29(13): 1542–1544.

152. A. Schliesser, M. Brehm, F. Keilmann, D.W. van der Weide. "Frequency-Comb Infrared Spectrometer for Rapid, Remote Chemical Sensing". Opt. Express. 2005. 13(22): 9029–9038.

153. L. Maidment, P.G. Schunemann, D.T. Reid. "Molecular Fingerprint-Region Spectroscopy from 5 to 12 μm Using an Orientation-Patterned Gallium Phosphide Optical Parametric Oscillator". Opt. Lett. 2016. 41(18): 4261–4264.

154. O. Kara, L. Maidment, T. Gardiner, P.G. Schunemann, D.T. Reid. "Dual-Comb Spectroscopy in the Spectral Fingerprint Region Using OPGaP Optical Parametric Oscillators". Opt. Express. 2017. 25(26): 32 713–32 721.

155. R. Salem, Z. Jiang, D. Liu, R. Pafchek, D. Gardner, et al. "Mid-Infrared Supercontinuum Generation Spanning 1.8 Octaves Using Step-Index Indium Fluoride Fiber Pumped by a Femtosecond Fiber Laser Near 2 μm". Opt. Express. 2015. 23(24): 30592–30602.

156. R.R. Gattass, L.B. Shaw, V. Nguyen, P. Pureza, I.D. Aggarwal, et al. "All-Fiber Chalcogenide-Based Mid-Infrared Supercontinuum Source". Opt. Fiber Technol. 2012. 18(5): 345–348.

157. Y. Yu, X. Gai, T. Wang, P. Ma, R. Wang, et al. "Mid-Infrared Supercontinuum Generation in Chalcogenides". Opt. Mater. Express. 2013. 3(8): 1075–1086.

158. E. Tournie, A.N. Baranov. "Mid-Infrared Semi-Conductor Lasers: A Review". Semicond. Semimetals. 2012. 86: 183–226.

159. S. Slivken, D. Wu, M. Razeghi. "Surface Emitting, Tunable, Mid-Infrared Laser with High Output Power and Stable Output Beam". Sci. Rep. 2019. 9(1): 1–7.

160. G. Veerabathran, S. Sprengel, A. Andrejew, M.-C. Amann. "Room-Temperature Vertical-Cavity Surface-Emitting Lasers at 4 μm With GaSb-Based Type-II Quantum Wells". Appl. Phys. Lett. 2017. 110(7): 071104.

161. S. Hofling, R. Weih, M. Dallner, M. Kamp. "Interband Cascade Lasers for the Mid-Infrared Spectral Region". In: Novel In-Plane Semiconductor Lasers XIII. USA: International Society for Optics and Photonics, 2014. Vol. 9002, P. 90021B.

162. Z. Du, S. Zhang, J. Li, N. Gao, K. Tong. "Mid-Infrared Tunable Laser-Based Broadband Fingerprint Absorption Spectroscopy for Trace Gas Sensing: A Review". Appl. Sci. 2019. 9(2): 338.

163. J. Hong, H. Kim, F. Shepherd, C. Rogers, B. Baulcomb, et al. "Matrix-Grating Strongly Gain-Coupled (MC-SGC) DFB Lasers with 34 nm Continuous Wavelength Tuning Range". IEEE Photonics Technol. Lett. 1999. 11(5): 515–517.

164. B. Mroziewicz. "External Cavity Wavelength Tunable Semiconductor Lasers: A Review". Opto-Electron. Rev. 2008. 16(4): 347.

165. J. Devenson, R. Teissier, O. Cathabard, A. Baranov. "InAs/AlSb Quantum Cascade Lasers Emitting Below 3 μm". Appl. Phys. Lett. 2007. 90(11): 111118.

166. J. Devenson, O. Cathabard, R. Teissier, A. Baranov. "InAs/AlSb Quantum Cascade Lasers Emitting at. 2.75–2.97μm". Appl. Phys. Lett. 2007. 91(25): 251102.

167. S. Kumar, B.S. Williams, Q. Hu, J.L. Reno. "1.9 THz Quantum-Cascade Lasers with One-Well Injector". Appl. Phys. Lett. 2006. 88(12): 121123.

168. C.J. Hawthorn, K.P. Weber, R.E. Scholten. "Littrow Configuration Tunable External Cavity Diode Laser with Fixed Direction Output Beam". Rev. Sci. Instrum. 2001. 72(12): 4477–4479.

169. M.G. Littman, H.J. Metcalf. "Spectrally Narrow Pulsed Dye Laser Without Beam Expander". Appl. Opt. 1978. 17(14): 2224–2227.

170. W. Hong, O. Painter. "Design and Characterization of a Littrow Configuration External Cavity Diode Laser". California Institute of Technology, 2004. http://web.mit.edu/rsi/compendium/edit2004/Final/hong-wenxian-caltech-both.pdf [accessed May 19 2021].

171. M.J. Baker, J. Trevisan, P. Bassan, R. Bhargava, H.J. Butler, et al. "Using Fourier Transform IR Spectroscopy to Analyze Biological Materials". Nat. Protoc. 2014. 9(8): 1771.

172. T. Wrobel, M. Kole, R. Bhargava. "Emerging Trends and Opportunities in Discrete-Frequency Infrared and Raman Spectroscopic Imaging". Spectroscopy. 2016. 31(6): 28–45.

173. Y. Phal, K. Yeh, R. Bhargava. "Polarimetric Infrared Spectroscopic Imaging Using Quantum Cascade Lasers". In: J.-X. Cheng, W. Min, G.J. Simpson, editors. Advanced Chemical Microscopy for Life Science and Translational Medicine. San Francisco, California; February 1–3, 2020. Vol. 11252, Pp. 36–45.

174. T.P. Wrobel, P. Mukherjee, R. Bhargava. "Rapid Visualization of Macromolecular Orientation by Discrete Frequency Mid-Infrared Spectroscopic Imaging". Analyst. 2017. 142(1): 75–79.

175. Y. Phal, K. Yeh, R. Bhargava. "Concurrent Vibrational Circular Dichroism Measurements with Infrared Spectroscopic Imaging". Anal. Chem. 2021. 93(3): 1294–1303.

176. W.L. Wolfe, P.W. Kruse. "Thermal Detectors". In: M. Bass, C.M. DeCusatis, J.M. Enoch, editors. Handbook of Optics: Volume II. Design, Fabrication, Testing; Sources and Detectors; Radiometry and Photometry. New York: McGraw-Hill Professional, 1995. Chap. 19, Pp. 19.1–19.14.

177. M.J. Riedl. Optical Design Fundamentals for Infrared Systems. Bellingham, WA: SPIE Press, 2001. P. 48.

178. L. Hoglund, C. Asplund, R.M. von Wurtemberg, A. Gamfeldt, et al. "Advantages of T2SL: Results from Production and New Development at IRnova". In: Infrared Technology and Applications XLII. USA: International Society for Optics and Photonics. 2016. Vol. 9819, P. 98190Z.

179. A. Rogalski. "Next Decade in Infrared Detectors". In: Electro-Optical and Infrared Systems: Technology and Applications XIV. USA: International Society for Optics and Photonics. 2017. Vol. 10433, P. 104330L.

180. A. Peterson-Greenberg, M.D. Pavel. "Laboratory Characterization of SLS-Based Infrared Detectors for Precision Photometry". In: High Energy, Optical, Infrared Detectors for Astronomy VIII. USA: International Society for Optics and Photonics. 2018. Vol. 10709, P. 107092C.

181. R. Ivanov, S. Smuk, D. Evans, W. Diel, D. Rihtnesberg, et al. "III-V Based Infrared Detectors Are Imposing New Standards". In: Infrared Technology and Applications XLVI. USA: International Society for Optics and Photonics. 2020. Vol. 11407, P. 114070Q.

182. A. Rogalski. "Infrared Detectors for the Future". Acta Phys. Pol., A. 2009. 116(3): 389.

183. A. Rogalski. "Infrared Detectors: Status and Trends". Prog. Quantum Electron. 2003. 27(2–3): 59–210.

184. L.J. Kozlowski, W.F. Kosonocky. "Infrared Detector Arrays". In: M. Bass, E.W. Van Stryland, D.R. Williams, W.L. Wolfe, editors. Handbook of Optics: Volume I – Fundamentals, Techniques, and Design. McGraw-Hill Professional, 1995. Chap. 23, Part 6, Pp. 1–25.

185. D.A. Scribner, M.R. Kruer, J.M. Killiany. "Infrared Focal Plane Array Technology". Proc. IEEE. 1991. 79(1): 66–85.

186. R.D. Hudson. Infrared System Engineering. New York: Wiley-Interscience, 1969.

187. P.R. Norton, J.B. Campbell III, S.B. Horn, D.A. Reago. "Third-Generation Infrared Imagers". In: Infrared Technology and Applications XXVI. USA: International Society for Optics and Photonics. 2000. Vol. 4130, Pp. 226–236.

188. P. Norton. "Third-Generation Sensors for Night Vision". Opto-Electron. Rev. 2006. 14(1): 1–10.

189. W.L. Wolfe. "Infrared Imaging Devices in Infrared Medical Radiography". Ann. NY Acad. Sci. 1964. 121: 57–70.

190. A.W. Hoffman, P.J. Love, J.P. Rosbeck. "Megapixel Detector Arrays: Visible to 28 μm". In: Focal Plane Arrays for Space Telescopes. USA: International Society for Optics and Photonics, 2004. Vol. 5167, Pp. 194–203.

191. S.B. Horn, P.R. Norton, K.R. Carson, R.C. Eden, R.E. Clement. "Vertically Integrated Sensor Arrays: VISA". In: Infrared Technology and Applications XXX. USA: International Society for Optics and Photonics. 2004. Vol. 5406, Pp. 332–340.

192. R. Balcerak, S. Horn. "Progress in the Development of Vertically Integrated Sensor Arrays". In: Infrared Technology and Applications XXXI. USA: International Society for Optics and Photonics, 2005. Vol. 5783, Pp. 384–391.

193. E.L Dereniak, G.D. Boreman. Infrared Detectors and Systems. New York: Wiley-Interscience, 1996. P. 24.

194. E. Hecht. Optics. Delhi, India: Pearson Education, 2002.

195. S. Mittal, K. Yeh, L.S. Leslie, S. Kenkel, A. Kajdacsy-Balla, et al. "Simultaneous Cancer and Tumor Microenvironment Subtyping Using Confocal Infrared Microscopy for All-Digital Molecular Histopathology". Proc. Natl. Acad. Sci. U.S.A. 2018. 115(25): E5651–E5660.

196. J.W. Goodman. Introduction to Fourier Optics. Englewood: Roberts and Company, 2005.

197. T. Wilson, C.J.R. Sheppard. Theory and Practice of Scanning Optical Microscopy. London, UK: Academic Press, 1984. P. 180.

198. J. Mertz. Introduction to Optical Microscopy. UK: Cambridge University Press, 2019.

199. C.J.R. Sheppard, T. Wilson. "The Image of a Single Point in Microscopes of Large Numerical Aperture". Proc. R. Soc. London, Ser. A. 1982. 379(1776): 145–158.

200. J. White, W. Amos, M. Fordham. "An Evaluation of Confocal Versus Conventional Imaging of Biological Structures by Fluorescence Light Microscopy". J. Cell Biol. 1987. 105(1): 41–48.

201. E. Abbe. "Beitrage zur Theorie des Mikroskops und der Mikroskopischen Wahrnehmung". Arch. Mikrosk. Anat. Entwicklungsmech. 1873. 9(1): 413–418.

202. L. Rayleigh. "Investigations in Optics, with Special Reference to the Spectroscope". Philos. Mag. 1879. 8(49): 261–274.

203. P. Lasch, D. Naumann. "Spatial Resolution in Infrared Microspectroscopic Imaging of Tissues". Biochim. Biophys. Acta, Biomembr. 2006. 1758(7): 814–829.

204. M.G. Gustafsson. "Surpassing the Lateral Resolution Limit by a Factor of Two Using Structured Illumination Microscopy". J. Microsc. 2000. 198(2): 82–87.

205. E.H. Rego, L. Shao, J.J. Macklin, L. Winoto, G.A. Johansson, et al. "Nonlinear Structured-Illumination Microscopy with a Photoswitchable Protein Reveals Cellular Structures at 50 nm Resolution". Proc. Natl. Acad. Sci. U.S.A. 2012. 109(3): E135–E143.

206. E. Narimanov. "Hyperstructured Illumination". ACS Photonics. 2016. 3(6): 1090–1094.

207. E. Narimanov. "Resolution Limit of Label-Free Far-Field Microscopy". Adv. Photonics. 2019. 1(5): 056003.

208. E. Betzig, G.H. Patterson, R. Sougrat, O.W. Lindwasser, S. Olenych, et al. "Imaging Intracellular Fluorescent Proteins at Nanometer Resolution". Science. 2006. 313(5793): 1642–1645.

209. M.J. Rust, M. Bates, X. Zhuang. "Sub-Diffraction Limit Imaging by Stochastic Optical Reconstruction Microscopy (STORM)". Nat. Methods. 2006. 3(10): 793–796.

210. T. Van Dijk, D. Mayerich, R. Bhargava, P.S. Carney. "Rapid Spectral-Domain Localization". Opt. Express. 2013. 21(10): 12822–12830.

211. S. Perrin, P. Montgomery. "Fourier Optics: Basic Concepts". arXiv preprint arXiv: 1802.07161. 2018. https://arxiv.org/pdf/1802.07161.pdf [accessed May 19 2021].

212. A. Daniels. Field Guide to Infrared Systems, Detectors, FPAs. Bellingham, WA: SPIE Press, 2010.

213. S.E. Reichenbach, S.K. Park, R. Narayanswamy. "Characterizing Digital Image Acquisition Devices". Opt. Eng. 1991. 30(2): 170–178.

214. J.K. Roland. "A Study of Slanted-Edge MTF Stability and Repeatability". In: Image Quality and System Performance XII. USA: International Society for Optics and Photonics, 2015. Vol. 9396, P. 93960L.

215. F. Van Den Bergh. "On the Rendering of Synthetic Images with Specific Point Spread Functions". In: Twenty-Third Annual Symposium of the Pattern Recognition Association of South Africa, 2012. P. 75. http://www.prasa.org/proceedings/2012/prasa2012-13.pdf [accessed May 19 2021].

216. F. Viallefont-Robinet, D. Helder, R. Fraisse, A. Newbury, F. Van Den Bergh, et al. "Comparison of MTF Measurements Using Edge Method: Towards Reference Data Set". Opt. Express. 2018. 26(26): 33625–33648.

217. J. Radon. "On the Determination of Functions from Their Integral Values Along Certain Manifolds". IEEE Trans. Med. Imaging. 1986. 5(4): 170–176.

218. P.D. Burns. "Slanted-Edge MTF for Digital Camera and Scanner Analysis". In: IS and T's Pics Conference. Society for Imaging Science and Technology. 2000. Pp. 135–138. https://www.imaging.org/site/PDFS/Papers/2000/PICS-0-81/1621.pdf [accessed May 19 2021].

219. R.C. Gonzalez, R.E. Woods, S.L. Eddins. Digital Image Processing Using MATLAB. India: Pearson Education, 2004.

220. K. Kohm. "Modulation Transfer Function Measurement Method and Results for the Orbview-3 High Resolution Imaging Satellite". In: XXth ISPRS Congress. Geo-Imagery Bridging Continents. Istanbul, Turkey; July 12–23, 2004. Vol. 25, Pp. 7–12. https://www.isprs.org/proceedings/XXXV/congress/comm1/papers/2.pdf [accessed May 19 2021].

221. J.L. Harris. "Resolving Power and Decision Theory". J. Opt. Soc. Am. 1964. 54(5): 606–611.

222. A. Santos, I.T. Young. "Model-Based Resolution: Applying the Theory in Quantitative Microscopy". Applied Optics. 2000. 39(17): 2948–2958.

223. C.E. Shannon. "A Mathematical Theory of Communication". Bell Syst. Tech. J. 1948. 27(3): 379–423.

224. L. Seidel. "Zur Dioptrik. Über die Entwicklung der Glieder 3ter Ordnung welche den Weg eines ausserhalb der Ebene der Axe gelegene Lichtstrahles durch ein System brechender Medien bestimmen, vo Herrn Dr. L. Seidel". Astron. Nachr. 1856. 43(19): 289.

225. D. Scaramuzza, A. Martinelli, R. Siegwart. "A Toolbox for Easily Calibrating Omnidirectional Cameras". In: 2006 IEEE/RSJ International Conference on Intelligent Robots and Systems. Beijing, China; Oct 9–16, 2006. Pp. 5695–5701.

226. R.R. Shannon. The Art and Science of Optical Design. UK: Cambridge University Press, 1997.

227. W.J. Smith. Modern Optical Engineering. New York: McGraw-Hill Education, 2008.

228. X. Sang, A.R. Lupini, J. Ding, S.V. Kalinin, S. Jesse, et al. "Precision Controlled Atomic Resolution Scanning Transmission Electron Microscopy Using Spiral Scan Pathways". Sci. Rep. 2017. 7: 43585.

229. Y.K. Yong, A. Bazaei, S.O.R. Moheimani, F. Allgower. "Design and Control of a Novel Non-Raster Scan Pattern for Fast Scanning Probe Microscopy". In: 2012 IEEE/ASME International Conference on Advanced Intelligent Mechatronics (AIM). Kaohsiung, Taiwan; July 11–14, 2012. Pp. 456–461.

230. R. Bhargava, D.C. Fernandez, M.D. Schaeberle, I.W. Levin. "Theory and Application of Gain Ranging to Fourier Transform Infrared Spectroscopic Imaging". Appl. Spectrosc. 2001. 55(12): 1580–1589.

231. K. Yeh, R. Reddy, R. Bhargava. "Fourier Transform Infrared Spectroscopic Imaging: An Emerging Label-Free Approach for Molecular Imaging". In: M.A. Anastasio, P. La Riviere, editors. Emerging Imaging Technologies in Medicine. Boca Raton, FL: CRC Press, 2013. Chap. 20, Pp. 322–351.

232. R. Bhargava, D.C. Fernandez, M.D. Schaeberle, I.W. Levin. "Effect of Focal Plane Array Cold Shield Aperture Size on Fourier Transform Infrared Micro-Imaging Spectrometer Performance". Appl. Spectrosc. 2000. 54(12): 1743–1750.

233. R. Westervelt, H. Abarbanel, R. Garwin, R. Jeanioz, J. Kimbel. Imaging Infrared Detectors II. McLean, VA: The MITRE Corporation, 2000. https://fas.org/irp/agency/dod/jason/iird.pdf [accessed May 19 2021].

234. P.G. Datskos, N.V. Lavrik. "Detectors: Figures of Merit". In: C. Hoffman, R.G. Driggers, editors. Encyclopedia of Optical Engineering. New York: Marcel Dekker, 2003. Vol. 1, Pp. 349–357.

235. A. Rogalski. "Progress in Focal Plane Array Technologies". Prog. Quantum Electron. 2012. 36(2–3): 342–473.